Design, Fabrication and Function Validation of a Myoelectric-Activated Torque-Controlled Robotic Rehabilitation Device

Author:

Marek Wartenberg

798329

Thesis Supervisor:

Professor Federico Casolo

Politecnico di Milano

School of Information Engineering

Automation & Control Engineering

2012-2013

Acknowledgements

I would first like to thank my Major Advisor Dr. Donald Peterson, whose background is traditional biomechanics. When I expressed to him my desire to relate robotics, he adamantly encouraged me to pursue my interests. There was no robotics courses offered at the University of Connecticut so Dr. Peterson again encouraged me to branch out. Because of this I took two Robotics Engineering courses at Worcester Polytechnic Institute, one of which was taught by Dr. Gregory Fischer. I would like to sincerely thank Dr. Fischer for his willingness to step on as a cross-institutional member of my advisory committee. Having an expert in medical robotics to assist in my transition to the field was invaluable. I would also like to thank Dr. John Bennett for being a part of my advisory committee. It was Dr. Bennett's questions to me which shaped his influence in this project. Each time we met he poised questions that I could not answer, compelling me to later dig deeper and grow as an engineer.

I would like to acknowledge Dr. Newton de Faria from National Instruments. I met with Dr. de Faria on several occasions because I viewed his input so highly. He not only happily met with me to discuss the project, but he also loaned me some of his personal equipment to use. I would like to thank Dave Kaputa of the Biomedical Engineering Program for his input and assistance with software design and LabVIEW programming. Additionally, I would like to thank Peter Glaude and Serge Doyon of the UConn School of Engineering Machine Shop for their assistance in assembly of the mechanical device. Both Jennifer Desrosiers and Lisa Ephraim in the Biomedical Engineering Main Office assisted me countless times, so I would like to acknowledge them as well. Throughout this process I received some sort of assistance from several students in the Biodynamics Lab at the UConn Health Center. Most specifically I would like to thank Eric Bernstein, Katelyn Burkhart and Tarek Tantawy. I'd like to thank Eric for his

willingness to stop what he was doing and show general interest in assisting me, and I thank Tarek and Katelyn for their help with the motion capture system. Additionally, I'd like to thank NASA and the Connecticut Space Grant Consortium for funding this project; also Dr. Peterson once again for suggesting that I apply for the CT Space Grant.

Finally, I´d like to thank Professor Federico Casolo of Politecnico di Milano and Professor Andres Diaz Lantada of Universidad Politecnica de Madrid (UPM). After completing most of the thesis work at the University of Connecticut, Professor Casolo gladly stepped on as my thesis advisor at Politecnico di Milano and assisted me to come up with additional research to conduct during my time in the EAGLES double degree program. This research, completed at UPM was generously hosted by Professor Diaz Lantada and for this I would like to acknowledge him.

Table of Contents

List of Figures

List of Tables

List of Annexes

Abstract

It is apparent that the future of limb rehabilitation will incorporate robotics alongside traditional physical therapy. Physical therapy is grounded in provoking motor neuron plasticity, traditionally by moving a patient's affected limb through balance and coordination exercises. Robots can be programmed precisely to move a limb through the same exercises with more repetition and intensity and individualized to the patient's needs. This thesis presents the successful design, fabrication, and validation of a novel myoelectrically-activated robotic rehabilitation device. In addition to a Myoelectric mode, there are Manual, Routine, and Master-Save modes that give the patient the aforementioned individualized rehabilitation opportunities. The overall device is a system consisting of a one degree of freedom robotic brace for each elbow that is intended to assist in the rehabilitation of hemiparetic patients. In the Myoelectric control mode, electromyography is read from both upper extremities and used as the metric of muscle output. Assisting the affected arm and resisting the unaffected arm as needed, the system guides myoelectrically-activated torque-controlled bilateral motions of both arms. The three additional control modes each provide a unique way for a patient's hemiparetic arm to be manipulated. The Manual mode allows for the program user to directly control the flexion and extension while the Routine mode oscillates flexion and extension continuously and in the Master-Slave mode, either brace can directly control the other via a master-slave algorithm. Data collected from an opto-electronic motion capture system and from outputs of the device were used to validate function of the different control modes. Validation showed that the braces provided a constant trajectory with very minimal, and consistent, lateral shift. Validations also showed that the Myoelectric control mode provided consistent outputs with respect to assisting or resisting affected and unaffected arms, respectively, but with an unexpected delay in motor activation and termination.

1. Introduction

Robotic therapy has been an increasingly developed technique for many applications. There are several benefits to robotic over traditional therapies that mainly focus on the ability to perform more precise and repetitive motions. Using robotic therapy alongside traditional methods has potential to increase not only the effectiveness of limb rehabilitation but increase the efficiency of the rehabilitation session. This project focused on rehabilitating elbow joint function in patients suffering from hemiparesis.

1.1 Hemiparesis

The term hemiparesis is often confused with hemiplegia, where hemiplegia is used to describe complete paralysis of one side of the body while hemiparesis refers to a weakened condition**.** Hemiparesis is most often caused by stroke and cerebral palsy and can also be caused by brain tumors, multiple sclerosis, and other diseases of the brain or nervous system. In fact, about 80% of people who have had a stroke have some degree of trouble moving one side or suffer from weakness on one side of their bodies. [9] The reason it generally affects one side of the body is that our brain is divided into two hemispheres with each hemisphere generally controlling the opposite side of the body; therefore, when one side is damaged, paralysis of the other side of the body occurs. [11] Children are susceptible as well, where brain damage can happen before, during, or soon after birth. In this case it is known as congenital hemiparesis or, if later in childhood, as acquired hemiparesis**.** [10] The causes of congenital hemiparesis are mostly unknown and usually parents become aware gradually during infancy, with increased risks in premature babies. [10] Regardless of age, other symptoms may be loss of speech, inability to swallow, urinary incontinence, memory loss, depression, or visual impairment.

The most notable quantification of hemiparesis is the Fugl-Meyer (FM) assessment scale. It had been used extensively and has great reliability. The scale accurately assesses total hemiparesis with a 98-99% sub-score and upper-extremity motor function with a 99.5-99.6% sub-score. [6, 21] The FM scale was initially developed to evaluate recovery from hemiplegic stroke. To accurately evaluate all effects, the scale is divided into 5 domains: motor function, sensory function, balance, joint range of motion, and joint pain. The quantification of upper limb motor function is a 66-point scale relating to the movement, coordination, and reflex of the shoulder, elbow, forearm, wrist, and hand, where each item is scored on a 3 point scale (i.e., 0 = cannot perform, 1 = performs partially, 2 = performs fully). [8, 27] For robotic devices that focus strictly on certain joint movement, it would be unnecessary to perform the full assessment on a subject. In addition, the 3-point scale for each movement may not prove useful for just one element because it does not distinguish between partial movements associated with hemiparesis. Therefore, future patient eligibility as well as rehabilitative outcomes may be better quantified using The Medical Research Council 6-point muscle strength scale (0 = no movement; 1 = flicker of movement; 2 = movement with gravity eliminated; 3 = movement against gravity; 4 = movement against resistance; 5 = full power). [8]

1.2 Traditional Therapy

Traditional therapy may be considered as methods used prior to the introduction of robotic assistance and is commonly thought of as physical therapists (PT) treating disabilities related to movement. They assist with strength, endurance, and range of motion problems. A PT will generally move a patient's affected limb through coordinated motions corresponding to everyday tasks. They can also help patients get back the use of weak arms and legs through coordination and balance skills exercises. [9] Traditionally, hemiparetic rehabilitation has been

emphasized during the first three months after onset, in accordance with studies of stroke recovery that show a plateau after three months. [2] This indicates that rehabilitation is most effective directly after brain injury.

Another form of traditional therapy is electrical stimulation, which has been used in the treatment of hemiparesis to strengthen the arm and improve range of motion. This procedure consists of placing small electrical pads on the weakened muscles of the arm and an electrical charge helps the muscles contract as the patient works to make it move**.** [9] Furthermore, treatments such as the injection of botulinum toxin (i.e., Botox) can improve this condition by stopping unwanted muscle contractions in a similar fashion to the mechanism employed to cosmetically avoid wrinkles. Another effective, but somewhat controversial technique is constraint-induced movement therapy (CIMT). This neuro-rehabilitation approach is designed to forcibly improve the use of an affected upper limb. The original therapy involves inducing the use of the affected limb by constraining the unaffected limb for up to 90% of waking hours over a two-week period, including two weekends. [23] This is controversial because, although it has proven to increase the strength and range of motion in the affected limb bilateral movements are encouraged to increase body symmetry and decrease abnormal tone in the early stages of rehabilitation. [2] In fact, several studies reported that repetitive bilateral arm training is effective in arm and hand motor recovery in stroke patients. [18, 26]

1.3 Movement to Robotic Therapy

In the last few decades focus has shifted to robotic rehabilitation. Robot-assisted sensorimotor rehabilitation was pioneered in the 1990's with the MIT-Manus, which was a device for training of arm recovery in stroke rehabilitation and can be seen below in Fig. 1. This

device adapts the timing and stiffness based on user's performance in a simple video game. [19] Studies with this device showed an increase in shoulder and elbow function when used alongside traditional therapy compared with patients who received strictly traditional methods.

Figure 1: MIT-Manus [19]

After this device proved robotic rehabilitation could be effective, countless other novel devices were prototyped and tested. The primary control method that has been explored so far is active assist robotic therapy, where the major goal of robotic therapy is provoking motor plasticity through precise and repetitive exercises to improve motor recovery. [19] Active assist exercise provides novel somatosensory stimulation that helps induce this brain plasticity. [15, 24 25] It is explicitly stated that robots can provide intensive training in a consistent manner without fatigue. [17] They can be used to manipulate the paretic arm by repetitive, high-intensity, task-specific movements. [20] As a PT would traditionally move a patients paretic limb through similar task-specific movements, robotic therapy allows much more repetition that can be programmed precisely, individualized, and adjusted according to the patient's needs. [17] It is also believed that a bilateral approach to robot-aided arm rehabilitation may offer a patient more

intensive practice opportunity without increasing the time the treating therapist spends in supervision. [2] In addition, using both arms gives a patient the ability to directly compare fully functional movements of their unaffected arm with the limited movements of their affected arm. This internal cognitive comparison could benefit the patient to understand what a motion "should" feel like and how to mimic that feeling on the opposite side.

Several other robotic devices for rehabilitation include the T-WREX (left) and the Pneu-WREX (right) shown below in Fig 2. The T-WREX uses passive gravity to assist, with the number of elastic bands determining that amount of assistance, while the Pneu-WREX creates a computer model of the patient's weaknesses and uses it to provide feed-forward assistance. [19]

Figure 2: T-WREX (left) and Pneu-WREX (right) [19]

An example of a bilateral device has been developed by [2]. The device is called a *bilateral force-induced isokinetic arm movement trainer (BFIAMT*) and can be seen in Fig 3**.** On the left is an image of the device, and the right is a picture of the device in use. As shown, the patients affected arm is bandaged to the handle. This device consists of two handles on a linear track which move in accordance to push and pull from the patient. The device requires the

patient to reach a specific bilateral force detected by load cells in order to initiate movement. Once the threshold is reached the system initiates movement in two servo motors to allow smooth motion of both handles symmetrically. As the patient increases their strength the set limit is raised requiring the patient to provide more force.

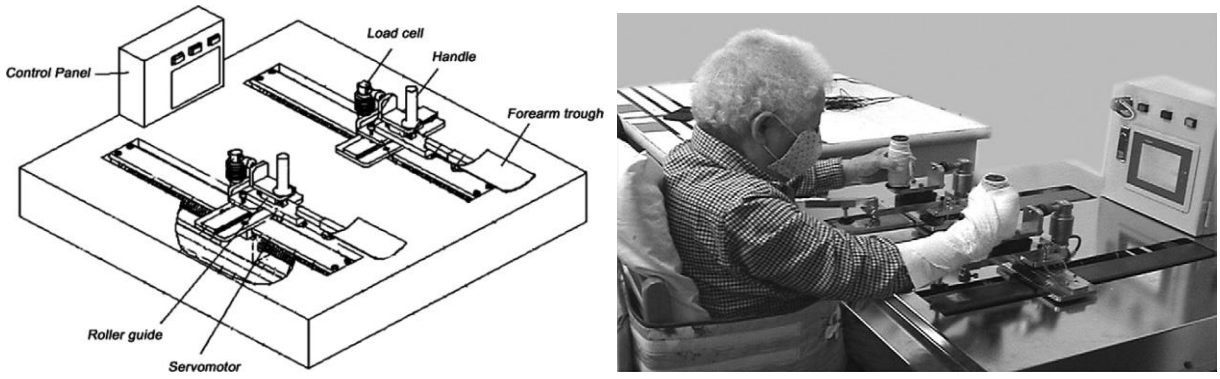

Figure 3:BFIAMT (left) BFIAMT in use (right) [2]

Similarly to the BFIAMT, the principal myoelectric control mode is meant to induce bilateral motion. This system relies on the level of muscle activation of the patient rather than using load cells to determine the force exerted.

Research exists that suggests guiding or assisting a movement may in fact decrease motor control learning for some tasks, where physically assisting a movement can change the dynamics of the task and what is learned is not the target but the assisted task. [19] For example, given an assistive robot which can “take over” a reaching task, several post-stroke patients decreased their own force output, letting the robot do more of the work of lifting their arm. Guiding or assisting the movement reduces the burden on the learner's motor system to perform the task successfully; therefore a commonly stated goal in active assist exercise is to provide "assistance-as-needed" rather than general assistance. [19]

1.4 Project Scope

This project focuses on rehabilitating the elbow joint of hemiparetic patients by stressing bilateral, symmetrical movements of both arms. Four distinct control modalities, Manual, Routine, Master-Slave and Myoelectric all allow for varied rehabilitative tasks. A robotic system was designed and fabricated to implement these controls. It is comprised of two mirrored devices, one for each elbow joint. The principal control mode reads Electromyography (EMG), the electrical activity of muscles during contraction, from both arms. Using this biosignal, the system assists the affected arm while resisting the unaffected arm using torque controlled motors to guidie bilateral arm movements. The current sent to the motor to provide necessary torque is directly calculated from the EMG levels of the patient, resulting in myoelectric control. The three additional control modes each provide a unique way for a patient's hemiparetic arm to be manipulated. One allows for a user to directly control the flexion and extension, while another to cycle through flexion and extension continuously and finally one to allow the unaffected arm to directly control the affected via a master-slave algorithm. Regardless of the control mode, the ultimate goal of this system is to stimulate motor neuron plasticity and re-innervate a hemiparetic arm. The system is calibrated for each patient and is adapted to account for all levels of hemiparesis. For the context of this system, the hemiparetic individual will always be referred to as the "patient" and the person operating the system will always be referred to as the "user." The scope of this project was to design, fabricate and validate function of this robotic rehabilitation device. Explicitly, personal contributions were design and fabrication of the mechanical device, writing the software code for each control modality, integrating software to the mechanical device via a National Instruments development platform and finally validation testing of all

components. Since the design and fabrication was a major portion of this project, the methods will contain the proposed design, and the results will show how that design was realized.

2. Methods

The work completed was designing, fabricating and validating function of a novel myoelectric controlled robotic rehabilitation device. This bilateral device was in effect two identical 1 DOF devices, mirrored for each arm. The 1 DOF corresponds to the elbow joint, in which motion would be assistive or resistive based on which arm is affected and the control method chosen. Four control modes were implemented: a Manual Control mode where the user controls the flexion and extension, a Routine mode which simply puts an affected arm through an indefinite repetition of flexion-extension cycles, a Master-Slave mode in which either arm can force the other to mimic its motion, and, finally, a Myoelectric control mode where the unaffected arm's flexion or extension will be resisted to correspond to motion in the affected arm. This final control mode guides the user to produce bilateral flexion-extension motions simultaneously. The system was developed using National Instruments (NI) (Austin, TX) hardware programmed in NI LabVIEW, which is a graphical programming environment where a user creates a Virtual Instrument (VI) with two main components, a front panel and a block diagram. The front panel is the user interface and typically consists of various controls and indicators. The block diagram is where the actual programming occurs, where these controls and indicators are connected via wires through a diverse assortment of function blocks. Examples of LabVIEW graphical programming used in this thesis work is in figures seen in later sections.

2.1 Hardware

The hardware chosen was the NI CompactRIO (cRIO), powered by reconfigurable input/output (RIO) Field-Programmable Gate Array (FPGA) technology. [24] The model chosen was the cRIO-9076 and can be seen in Fig. 4.

Figure 4: cRIO-9076

(Picture from http://sine.ni.com/ds/app/doc/p/id/ds-354/lang/en)

The chassis consists of a Real-Time (RT) Module and associated user-programmable FPGA, both explained in detail in the thesis. The chassis has four slots with the ability to accept a variety of hot-swappable function modules based on the necessity of the user. Each module and its function will also be described shortly but Fig. 5 illustrates how the different hardware components interact.

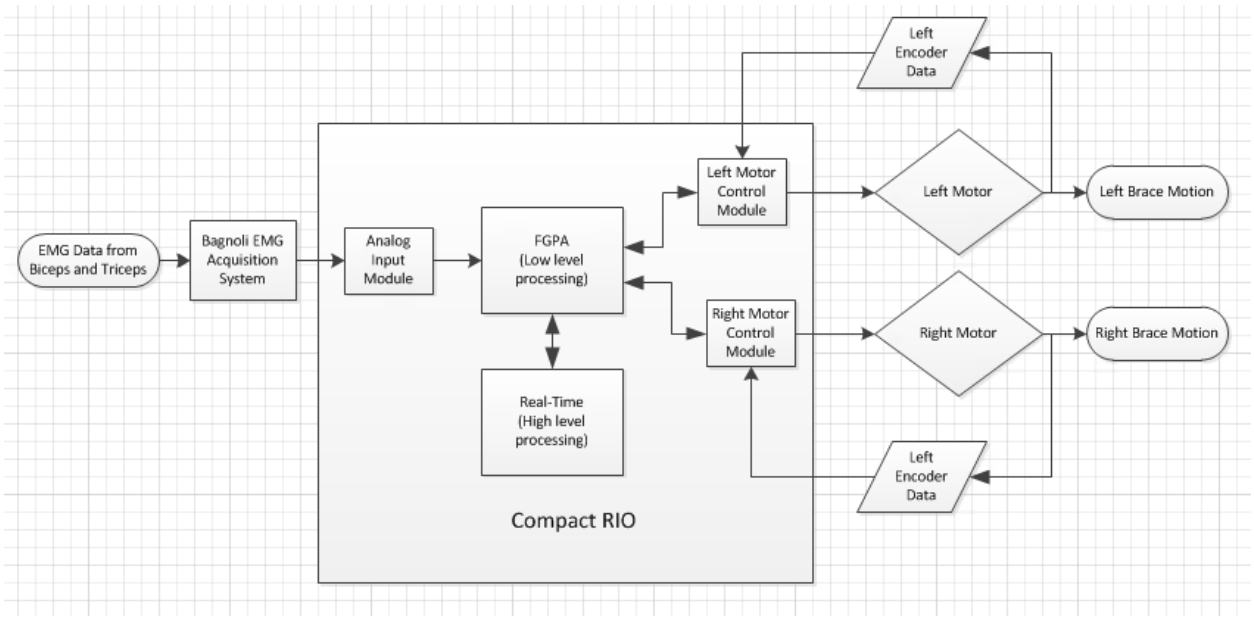

Figure 5: Hardware Flowchart

The FPGA interfaces directly with the swappable modules and the RT Module communicates with the FPGA. This device connects to the computer via crossover (Ethernet) cable and an application using this hardware can simultaneously run code from the host computer, RT Module and the FPGA. In the future this particular project will be a stand-alone or "headless" system, meaning it will only be programmed in the RT controller and FPGA, so the host computer component was left out in the above figure. Looking forward, programming only in these two locations will allow the system to be unplugged from the host computer and ultimately run autonomously. The hierarchy of this type of programming can be visualized in Fig. 6 below.

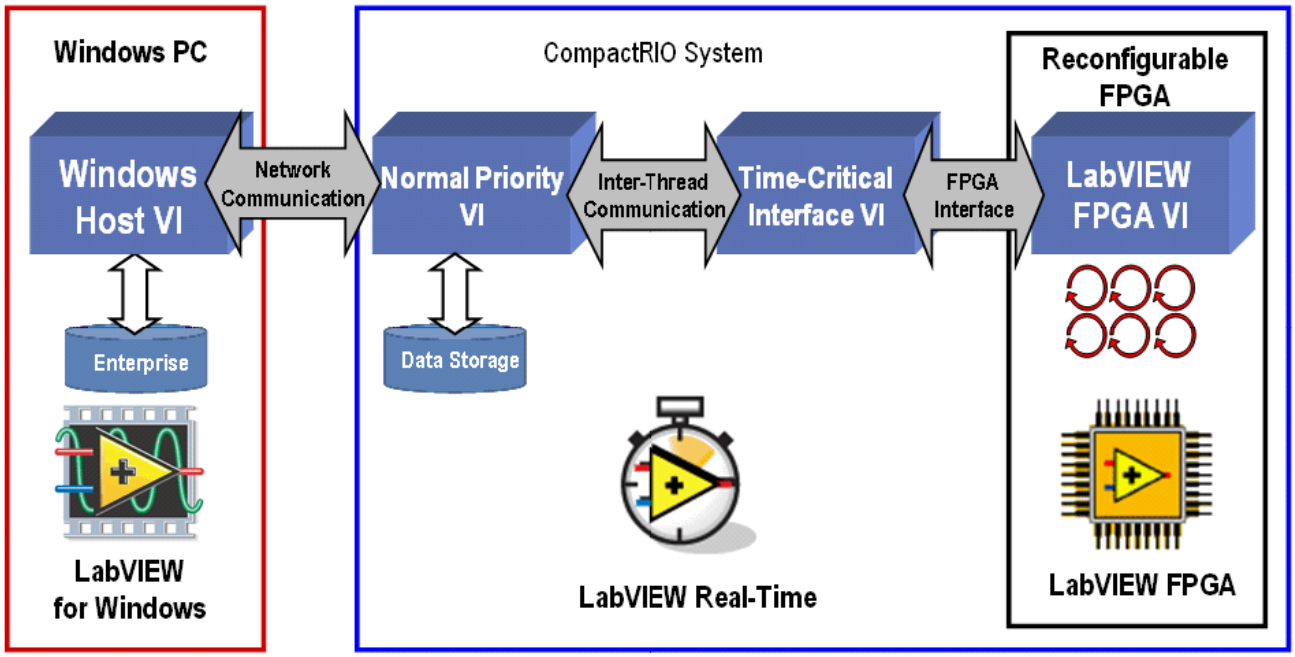

Figure 6: VI heirarchy and communication pathways for the cRIO system

(Picture from http://www.ni.com/white-paper/3261/en)

2.1.1 Real-Time Module

RT control is essential in creating stand-alone embedded systems. Traditional LabVIEW applications running on operating systems such as Windows are not optimized to run for extended periods of time. [25] The real-time operating systems (RTOS) allows for a stand-alone, "headless" system to run critical applications for prolonged lengths of time. It is important to note that "Real-Time" does not necessarily mean really fast; rather, it means absolute reliability of a deterministic system with timing constraints that must be met to avoid failure. [13] Determinism is the ability to complete a task within a fixed amount of time and a deterministic system is one which is bounded by this constraint. For example, a RT controller is needed deploy an airbag properly. The status of the airbag's state of inflation is not being continuously

monitored in “real-time,” but when it is initiated to deploy it must do so in a fixed amount of time or else it’s useless. This is a deterministic system requiring absolute reliability.

Referring back to traditional LabVIEW applications, the same graphical programming techniques are used in the RT Module; in fact the program is essentially written on the host PC then deployed onto the RTOS. There are hundreds of prewritten LabVIEW libraries that can run on the RT Module identically to a host PC based VI. [25] In this case all of the high-level processing will be done in the RT module rather than the PC, since this system will be made “headless” in the future.

As shown in the previous figure, the RT Module interfaces with, and is the intermediary between, the host PC and the FPGA. As the individual function modules only communicate with the FPGA, it is imperative to understand the hierarchy of data flow between the separate VI’s running on different targets. The FPGA and the RT are the two levels of programming used in this application where the FPGA is considered to be the lowest level in the VI hierarchy followed by the RT controller, and finally, the host PC. The FPGA is programmed with parallel “while” loops and any indicator or control can be read from or written to using the “Read/Write” block. This block is found in the RT VI, corresponding to the previously mentioned statement that the RT controller is the intermediary and needs to communicate to the FPGA directly.

2.1.2 FPGA Integrated Chassis

As mentioned, FPGA stands for Field-Programmable Gate Array. The particular model chosen for this application, the cRIO-9076 shown previously, combines the RT controller and FPGA into a more cost-effective single unit. More powerful models have these items sold separately with each having varying degrees of performance and ruggedness. This allows the

user to mix and match based on their application. In addition, both a four- and eight- slot chassis are available. Unlike the RT Module, the FPGA does not have an operating system because the code is implemented directly into the hardware. The gate-arrays are reprogrammable silicon chips, where programming an FPGA rewires the chip itself to implement desired functionality. [24]

Typical FPGA tasks include I/O, hardware-based triggering and low-level signal processing. Benefits of using FPGA technology include but are not limited to: Faster I/O response times, exceeding computer power of digital signal processors and implementing custom functionality with the reliability of dedicated deterministic hardware. [24] A general idea of FPGA architecture is shown in Fig. 7. It consists of configurable logic blocks (CLB), configurable I/O blocks and programmable interconnect to route signals in between. [1]

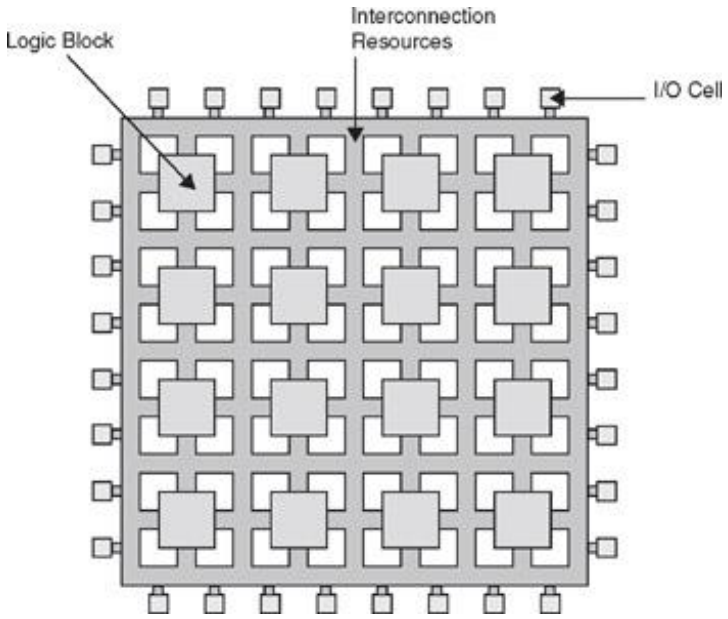

Figure 7: FPGA Architecture

(Picture From http://www.globalspec.com/reference/81250/203279/chapter-29-field-programmable-gate-arrays-fpgas)

First, the CLBs contain the actual programmable logic for the FPGA. A typical CLB contains RAM to create any combination of logic functions and it also contains multiplexers to route logic within the block as well as external resources. Next, the configurable I/O blocks have the power to bring signals onto the chip and send them back off again. This corresponds to the physical I/O on specific function modules chosen by the user to fill the slots of the chassis. Finally, the programmable interconnect links everything together in three distinct ways. [1] First, all CLBs are directly connected to each of their neighboring CLBs. These connections, commonly called *short lines* allow for complex logic that cannot fit into one CLB to be mapped across several. Another way the interconnect routes between CLBs is through switch matrices. Certain traces pass by several blocks before entering the switch matrix, which by name's description switches connections between different traces. This technique allows for physically distant CLBs to be integrated but potentially poses a problem because of the delay encountered at every switch matrix. Lastly the third interconnect type, called the *long line*, typically travels from one end of the FPGA to the other, without passing through a switch matrix. This allows for those physically distant CLBs to be interconnected without delay.

2.1.3 Analog Input Module

The first function module to be described is the Analog Input Module (model number NI 9215) This module has four simultaneously sampled analog inputs with input range at +/- 10V. This module has a 16 bit resolution ADC and accepts signals through BNC connection. It can be seen in Fig. 8.

Figure 8: NI 9215 Analog Input Module

(Picture from http://sine.ni.com/ds/app/doc/p/id/ds-73/lang/en**)**

2.1.4 Brushed Servo Drive Modules

Two of these modules were necessary, one for each motor in the system. These modules, model number NI 9505 as seen in Fig. 9, are full H-bridge brushed DC servo drives with direct connection to both the power source and actuation. It also contains a D-SUB connection for encoder feedback. Figure 8 shows the modules. There are several functionalities of this module that make it perfect for motor control in this application. For instance, the current-torque control allows for direct input of how many amps to deliver. This particular functionality proved imperative for the Myoelectric control mode, where the torque to be delivered is proportionally calculated from the level of EMG activation.

Figure 9: NI 9505 Brushed Servo Drive Module

(Picture from http://sine.ni.com/nips/cds/view/p/lang/en/nid/202711)

2.1.5 Digital I/O Module

The digital I/O module was used strictly in the testing and validation phase of the project, since there were no design functions that rely on this module to work. Instead, it was used to signal an output when the motors began to actuate. The details of this are described further in the Myoelectric control function validation section (section 3.4.3) The digital I/O module also accepted BNC input and looked essentially identical to the analog input module shown in Fig. 8.

2.2 Mechanical Design

The mechanical system is comprised of two individual devices identical in appearance and functionality except that they are simply mirrored images of each other. Identical bilateral devices allow for indiscrimination between persons with left- or right- side affected hemiparesis. The device was designed in SolidWorks (Waltham, Massachusetts) and the complete design along with an annotated exploded view is shown in Fig. 10. As these are essentially identical, only one is described and it is left to the reader to understand that there was a duplicate mirrored device fabricated simultaneously. The transparent support component, just like the other two, was rapid prototyped out of Polycarbonate using a process called Fused Deposition Modeling (FDM). It is important to note that the actual piece is not transparent, but was depicted this way in the model to show the drive train within.

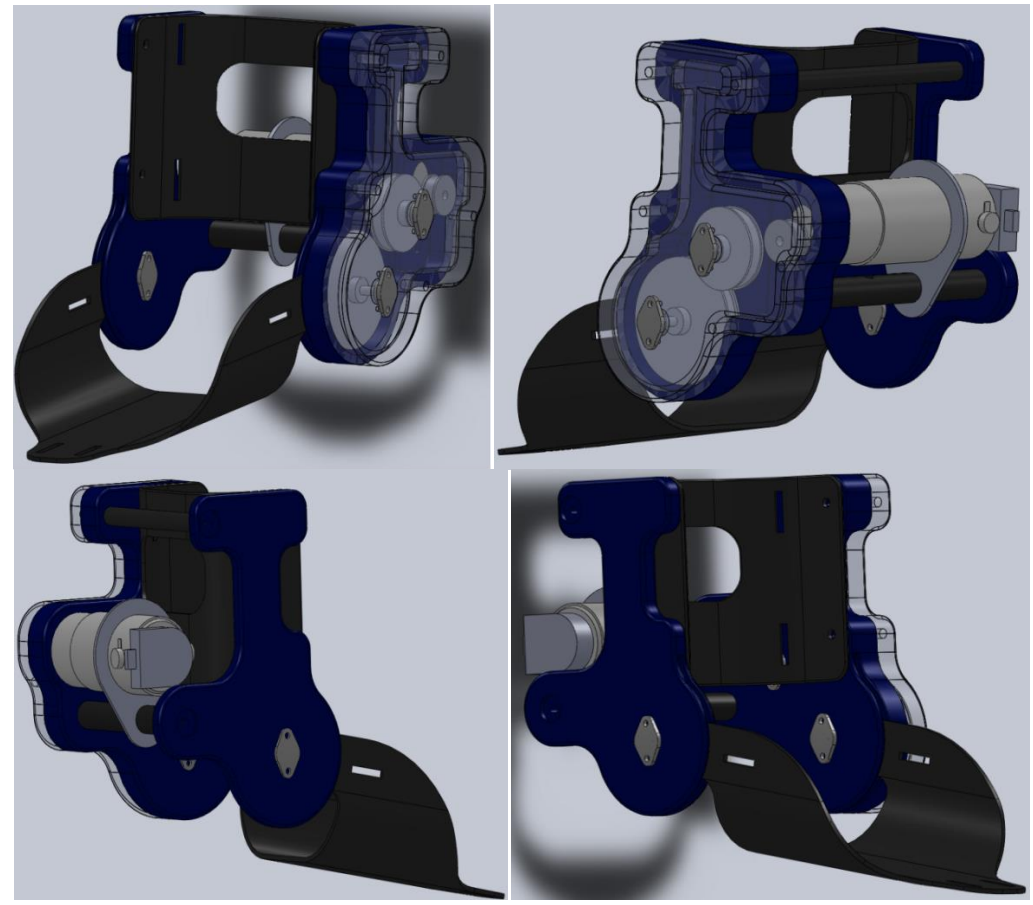

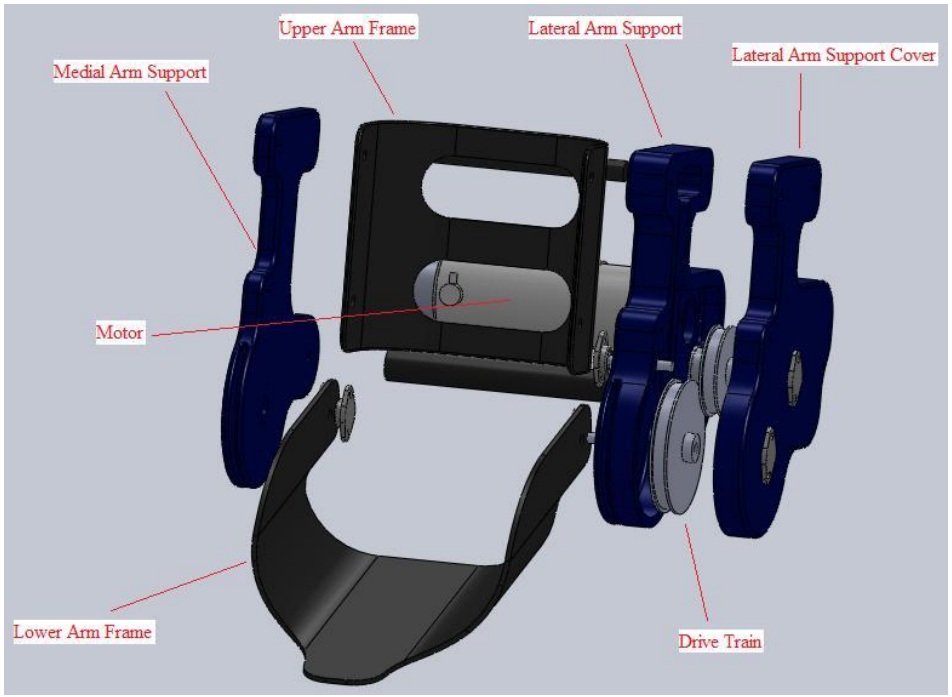

Figure 10: Mechanical design created in SolidWorks

2.2.1 FDM Rapid Prototyped Models

The device required three pieces to be rapid prototyped and once the designs were complete in SolidWorks, they were sent to Quickparts Inc. (Atlanta, GA) to complete this process. Rapid Prototyping, commonly called 3D printing, broadly refers to several mechanisms of creating custom extrusions from a variety of different plastic materials. It was pioneered in late 1980's with Stereolithography (SLA) but has since evolved into several much more powerful processes. [33] SLA, for instance, is great for fit and form testing but a much stronger process is required for functional prototypes. [32] There are several different mechanisms of 3D printing and the major differences between these processes include applications, layer thickness, material and finishing options, minimum feature size, and, most importantly, cost.

The rapid prototyping process chosen for this project was Fused Deposition Modeling, since it is ideal for conceptual models, engineering models, and functional testing prototypes. During FDM in particular, the plastic is melted and then extruded onto a platform to create a two-dimensional cross section of the model. This solidifies quickly then the platform descends and the process is repeated to create the next layer. [32] This process provides unrestricted design options. For example, if a hollow region is required, the machine can lay filler instead of material and then the filler can be dissolved post-production. Using FDM, several different materials can be chosen. The available materials and their respective mechanical properties can be seen in Table 1 and the chosen material, Polycarbonate, is highlighted. Polycarbonate was chosen primarily because of its mechanical properties and cost. Through discussion with the advisory committee and technicians at Quickparts, Polycarbonate was decided to produce the best cost to mechanical property ratio, without sacrificing functionality.

Table 2: FDM material choices and their mechanical properties

(Table from http://www.quickparts.com/LowVolumePrototypes/FDM/MaterialProperties.aspx)

Mechanical Properties	Tensile Strength	Tensile Modulus	Tensile Elongation at Break	Flexural Strength	Flexural Modulus	Heat Deflection (HDT)	Izod Impact, Notched
Test Method	ASTM D638	ASTM D638	ASTM D638	ASTM D790	ASTM D790	ASTM D648	ASTM D256
Units	psi	psi	%	psi	Psi	ºF	(ft-lb)/in
ABS	3200	236000	0.06	6000	266000	205º	2
Polycarbonate	7600	290000	0.03	14000	310000	260º	1
PC/ABS	5040	265000	0.043	8600	270000	205º	2.3
ABSi	5400	277700	0.031	8830	264000	188º	1.9
ABS-M30	5200	350000	0.04	8800	336000	204º	2.6
ABS-M30i	5200	350000	0.04	8800	336000	204º	2.6
PC-ISO	7500	253000	0.05	11830	318000	260º	1
ULTEM	10390	322000	0.059	n/a	362600	320º	2
PPSF	8000	300000	0.03	15900	320000	372º	1.1

The first piece described is the Lateral Arm Support, shown in Fig. 11. This can be considered the "anchor" of the whole device. This is the biggest of the rapid prototyped pieces and houses the drive train and interfaces directly with the motor.

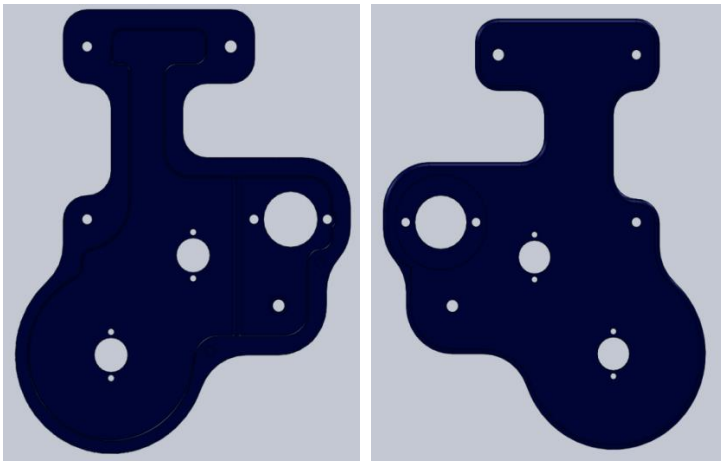

Figure 11: Lateral Arm Support

The largest hole with two smaller holes on either side is where the motor interfaces. The motor has two face-mount screw holes and the two holes on the side of the large one correspond to these. The two similar sized holes with smaller holes above and below them are for the mounted bearings. The bearings hold the shafts in place to rotate freely. The other four similar sized holes are strictly for assembly.

Next is the Lateral Arm Support Cover, which encloses the drive train and has similar mounted bearings to hold the jack shafts in place. When together, the two pieces are 1.72 inches thick. The cover is shown in Fig. 12.

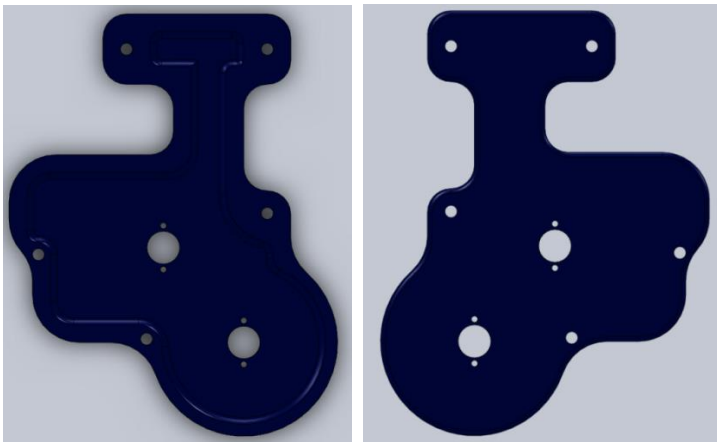

Figure 12: Lateral Arm Support Cover

This last piece to be described is the medial arm support, shown below in Fig. 13, which is 0.5 inches thick and sits between the arm and body of the user. This piece strictly serves as support and is anchored to the rest of the device via the two crossbars in the back and the aluminum arm frames.

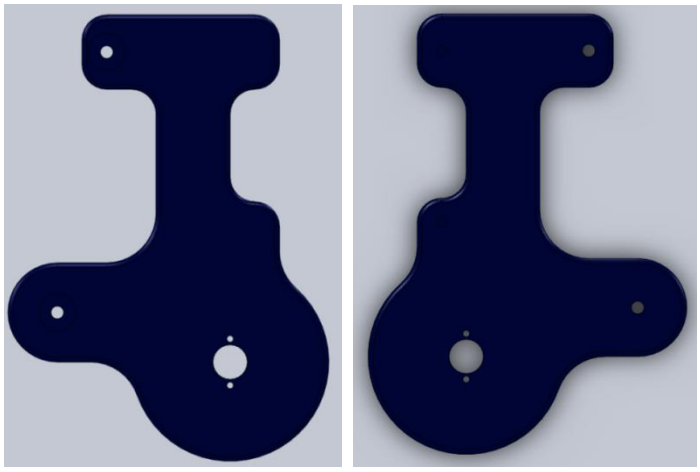

Figure 13: Medial Arm Support

2.2.2 Arm Frames

The other major support components were the arm frames between the support pieces. These were machined from a 1/8th inch thick aluminum sheet and bent on a hydraulic press using a pipe to create a smooth radius. The SolidWorks model of the pieces is illustrated in Fig. 14.

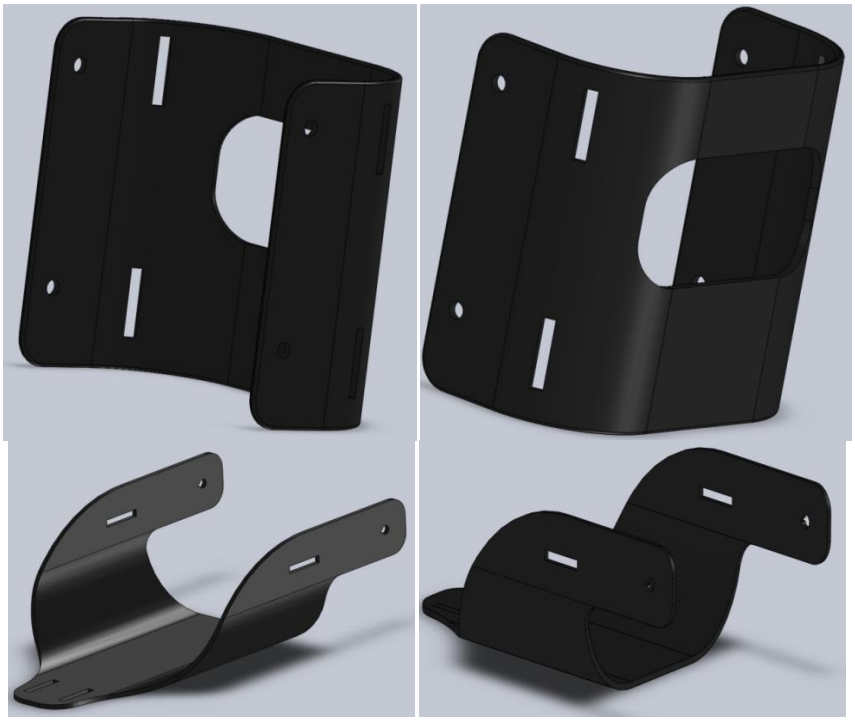

Figure 14: Aluminum arm frames

The two SolidWorks designs on top of Fig. 14 are of the upper arm frame, while the two on bottom are of the lower arm frame. The circular holes are attachment points and the thin slits are for the Velcro straps. The lower arm frames pivot on their attachment points while the upper arm frame is securely fastened in place. The large hole in the back on the upper arm frame is for EMG electrode access to the triceps.

2.2.3 Actuation

The motor was selected based on requirements for assistance and resistance of arm flexion and extension. It was understood that resisting arm flexion in the unaffected arm would require the most torque, and simple experiments with a torque wrench yielded an approximate requirement of 700 lb-in. This motor comes from Pittman Motors (model number GM14904S010 Lindale, TX) and comes with a built in encoder. The motor can be seen in Fig. 15. The motor itself has an internal gearbox with a gear ratio of 5.9:1 and is rated for 12V with full load amps reaching 5.91A. The no load speed of the motor is 597 rpm and the max continuous torque is 124 oz-in. The drive train to be described next increased this to the requirement for resisting arm flexion. The associated encoder is of single-ended type where all signals are commonly grounded.

Figure 15: Motor

(Picture from http://www.automationexpress.com/Products/DC_Motors/Images/GM14904S010.gif)

2.2.4 Drive Train

A two-step pulley and timing belt train was designed to transfer the motor output to the elbow for rotation. This pulley system can be seen in the close-up image in Fig. 16. It was originally planned to use gears but spanning the required distance between the motor and elbow with reasonably sized gears proved impossible; therefore, pulleys and belts were used instead. The views of Fig. 16 show the two step system. Although, in the straight on view, it looks like the middle and large pulleys interact, they are in fact off center and move independently. The large pulley interacts with the small pulley on the same shaft as the middle pulley and is behind the middle pulley in the figure.

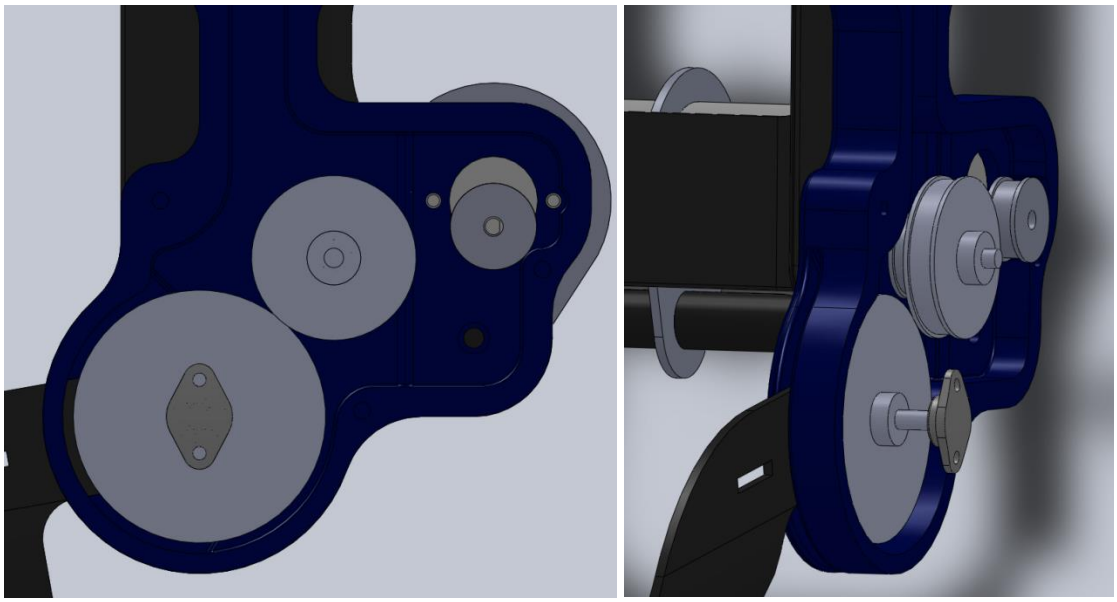

Figure 16: Pulley and belt drive train system

2.2.5 Safety

Several safety mechanisms were incorporated to ensure no harm comes to any patient. First, the amount of torque can be limited directly in the program, so the assisting or resisting torque to be given will never exceed what the treating therapist chooses. Also the patient's arm is strapped in securely with Velcro straps. The arm sits comfortably in the foam padding which protects and cushions the arm from the metal arm frames. Alignment of the elbow is also very important, and several thicknesses of foam padding for both the upper and lower arms allow for correct placement of the elbow along the axis of rotation. The most important safety measure to be taken is to avoid hyperextension of a patient's elbow. To account for this a mechanical hard stop was implemented into the design so the arm can only reach extension, not hyperextension. Also, full extension is characterized by the zero position for the encoders, so code was added to disable the motors if the encoder drops below zero. The hard-stop is illustrated in Fig. 17. The outline shows the cutout within the FDM model that is available for movement of the arm frames. It is impossible for the arm frames to move outside of this therefore eliminating the possibility of hyperextension.

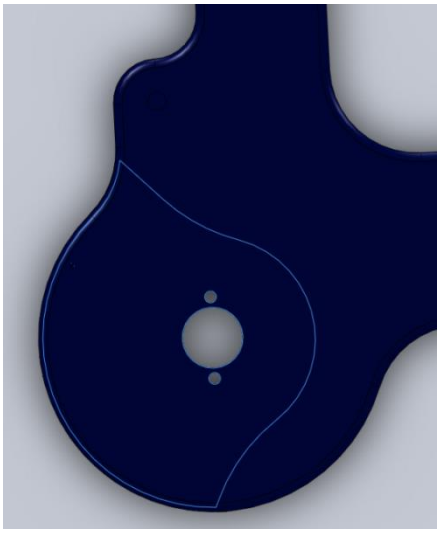

Figure 17: Mechanical hard stop

2.3 Electromyography

EMG is the signal used for motor actuation in the myoelectric control mode. EMG is the electrical activity of muscles during contraction where Fig. 18 shows an example of an EMG signal. There is very little electrical activity while the muscle is at rest but, during muscle contraction, the activity greatly increases. EMG stays at a particular baseline and simultaneously increases both positively and negatively during contraction.

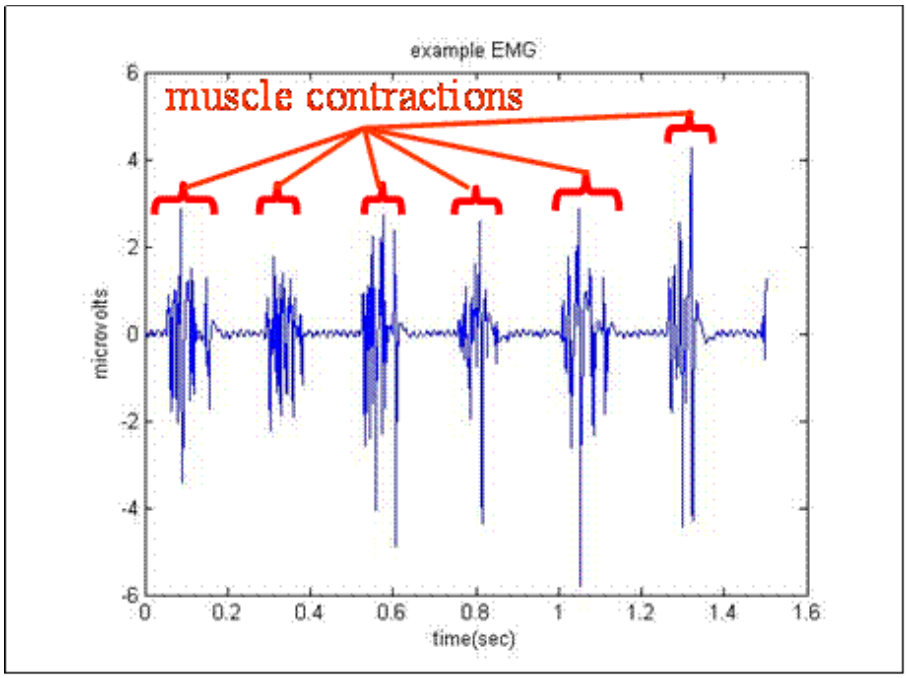

Figure 18: Typical EMG signal

(Picture from http://podiatry.temple.edu/gaitlab/facilities/images/emg_1.gif)

2.3.1 Acquisition

The EMG signals are captured from the biceps and triceps of each arm using a pair of Delsys Bagnoli Handheld EMG systems (Boston, MA). Each Bagnoli system has two channels

and one unit was dedicated to each arm. The handheld system is shown below in Fig 19 and each has two channels and can output through BNC connections to the cRIO.

Figure 19: Bagnoli Handheld EMG System

(Picture from http://www.delsys.com/Images/Bagnoli2.gif)

The electrodes associated with this system are reusable single differential detection sensors having a contact material of 99.9% Silver (Ag) arranged in a parallel-bar geometry for signal consistency. [5] Figure 20 shows a close up of this electrode and associated dimensions of the contact material. The electrodes require no gel or skin preparation; rather, a disposable adhesive interface simply sticks to the electrodes and skin. [5]

Figure 20: DE-2.1 Single Differential Detection Surface EMG sensor

(Pictures from http://www.delsys.com/Images/de21.gif(left) http://www.delsys.com/Images/electrodeperspective.gif (right)

The placement of the electrodes for each muscle was in accordance with the Surface EMG for the Non-Invasive Assessment of Muscles (SENIAM) project (www.seniam.org). The optimal placement for the bicep and triceps electrodes is shown in Fig. 21. The dots signify the origin and insertion points of these muscles while the "X" shows optimal placement of the electrode.

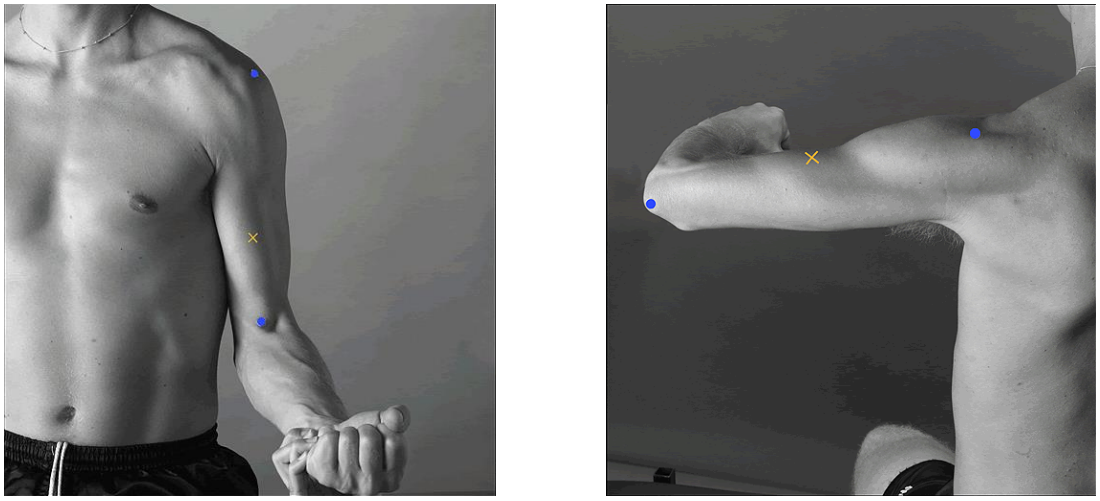

Figure 21: SENIAM suggested placement for surface EMG sensors on the bicep and triceps

(Pictures from http://www.seniam.org/images/SEMGlocations/ArmHandLoc01_large.gif (Left)

http://www.seniam.org/images/SEMGlocations/ArmHandLoc03_large.gif (Right)

2.3.2 Filtering and Amplification

Several myoelectric sampling rates and filter cutoff frequencies have been suggested by various studies. For instance, Lopez et al. [18] used a bandpass filter (10 Hz to 500 Hz) with a sampling rate of 1 KHz and **s**uggested against using a power line notch filter. Li et al. [16] used a bandpass filter (20 Hz to 500 Hz) as well, but included a 50 Hz notch filter to eliminate power line interference. They also showed that a much smaller pass band and lower sampling rate may provide sufficient data without losing excessive accuracy. Li et al. also indicated that almost all

previous applications of EMG pattern recognition-based control used a high-pass cut-off frequency ranging from 5 Hz to 20Hz [2, 5, 12, 16]. In addition, they noted that 1 KHz was a widely used sampling rate. Li et al. attempted to explain that cable noise, which is considered as one of several motion artifacts, can produce frequency components in the 1-50 Hz range and that electrode shift can produce frequency components of up to 20 Hz. They suggested that a typical range of high-pass cut-off frequency could capture much of this noise. Li et al. go on to state that lower frequency components of EMG spectrum primarily contain the information on the firing rates of active motor units. Although this information could be useful, it is not necessary to quantify movement and can be neglected if it would also eliminate signal components from motion artifacts and electrode shift. This study showed that using a high pass cut-off 60 Hz could be beneficial because it simultaneously eliminated the effects of motion artifacts and power line interference. They suggest a band pass filter of 60Hz to 250Hz for the conditioning of EMG signals. These suggestions were all tried and used as guidance and the final filter characteristics chosen are presented in the results section (Section 3.2.2).

Finally, Li et al. show that lowering the sampling rate from 1 KHz to 500 Hz is also beneficial. Halving this sampling rate saved 50% of memory storage and reduced processing time by 50%, while only reducing accuracy of movement identification by approximately 2%. The Bagnoli EMG system can amplify the signal 100, 1,000 and 10,000 times and has an inherent analog bandwidth of 20 to 450 Hz.

2.3.3 Conditioning

Once the signal has been filtered, it needs to be conditioned into a useable form. For the device to function efficiently, proper features must be extracted from the signal. Feature extraction is essential because it allows for characteristic elements of the signal to be exploited.

If an element consistently occurs in an EMG signal and is representative of a specific movement, it can be evidence of the user's intentions. The success of any pattern recognition problem depends almost entirely on the selection and extraction of features. [26] The target feature of this system is mean absolute value (MAV). Prior to continuous sampling, the user is asked to provide a maximum voluntary contraction (MVC) for both muscles of each arm. All incoming data is normalized using the respective MVC. Also, it is widely accepted to full-wave rectify the signal by simply taking the absolute value of it. As stated, the target feature MAV will be used to estimate muscle contraction. The MAV is defined in Equation 1 below.

$$MAV(k) = \frac{1}{k} \sum_{j=1}^{k} abs\big(emg(j)\big) \qquad \text{Eq. 1}$$

In the above equation $emg(j)$ stands for the j-th sample from the beginning of the experiment and k is the current sample. This equation can be modified to be applied recursively to a growing set of data. The modified recursive MAV is shown in Equation 2 and can be updated for a set of growing data.

$$MAV(k) = \frac{k-1}{k} MAV(k-1) + \frac{1}{k} MAV(emg(k)) \qquad \text{Eq. 2}$$

Although continuous data will be acquired, segments of the data will be processed one at a time. To efficiently filter and condition the signals, the waveform must be segmented and processed in order to determine the MAV from each segment. As with sampling rate and filter cut-off frequencies, different segment lengths have been proposed by different research groups. It is clearly stated in the literature that it must fall below the 300 ms requirement for acceptable

delay but remain large enough to maintain feature characteristics. [4, 12, 20] An issue can arise due to the delay in processing a segment. The first technique of segmentation considered was adjacent windowing, which is shown in Fig 22. In this technique, each segment is the same length and the window is increased by an amount equal to its size. [6]

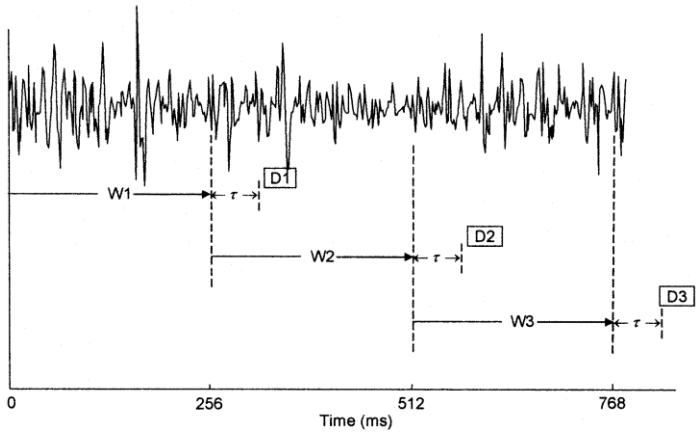

Figure 22: Adjacent windowing technique [6]

In Fig. 22, the processing delay, τ, is shown and each delay ends in a respective decision (D1, D2, and D3). This technique works but can be considered flawed because processing only occurs for a portion of the time spent acquiring data. This is inefficient use of processing capabilities and is why an overlapped windowing technique was introduced. In the overlapped windowing technique a new segment slides over the current segment with an increment of time less than the segment length. For efficiency, the length of overlap time corresponds to the length of the processing delay**.** This overlapped technique is illustrated in Fig. 23.

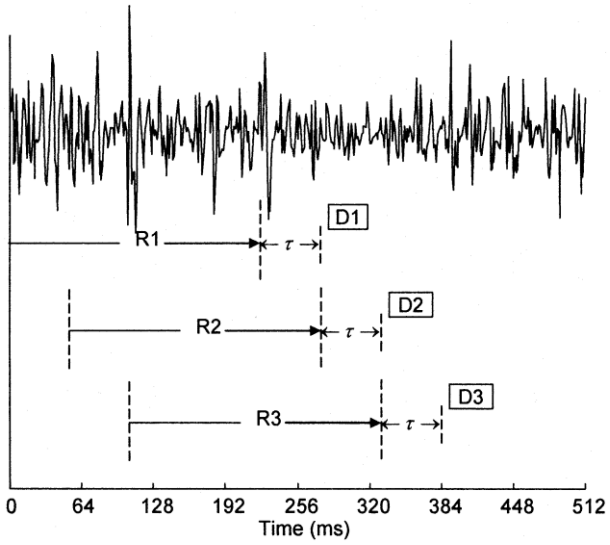

Figure 23: Overlapped windowing technique [6]

It is easily seen from Fig. 23 that, directly after the first segment is acquired, processing time, τ, occurs simultaneously while acquiring upcoming segments. As soon as the decision is made, the next segment is finished and processing immediately begins. In this case, a smaller segment would produce a more-dense but semi-redundant stream of decisions. [26] A larger segment could provide greater classification accuracy because of the statistical variance of features but increased segment size leads to increased processing time before a decision can be made. [6]

2.4 Control

There are four unique control mechanisms for this device. The first is Manual Control mode, where any user running the program can simply control flexion and extension or either arm with toggle switches on the LabVIEW front panel. The second is a simple Routine mode, where the arm is put through continuous cyclic flexion-extension motions. The third is a Master-Slave mode, where either side can control the other. This control mode allows for a user to flex

their unaffected arm and the device will automatically flex the affected arm. The final and most important mode is the Myoelectric controlled assistive-resistive mode, where the EMG signals are read from the biceps and triceps of both the affected and unaffected arms.

2.4.1 Manual

This is the most basic control mode. The person running the program can control flexion and extension of the patient's arm with toggle switches on the front panel of the VI, where up would reflect flexion and down would reflect extension.

2.4.2 Routine

The Routine mode is almost as basic as manual control. This simply oscillates the flexion and extension cycles of the affected arm. The program user can start and stop the cycles with the press of a button on the front panel and select which arm will cycle through the routine.

2.4.3 Master-Slave

In this mode the devices are on both arms and the unaffected limb is flexed and extended normally. The motor on the affected arm's device follows the motion of the unaffected arm, providing a way for a patient to indirectly control the flexion and extension of their affected arm immediately after it is damaged. Not only this, the therapist could wear the master brace and control the motion of the patient's arm just as they would when manually moving a patients arm. This was accomplished by programming one of the motors to follow the encoder value of the other.

2.4.4 Myoelectric

The essence of this modality is to guide the user to perform bilateral motions simultaneously. The EMG acquired from the affected arm would give information relating to the muscle effort of flexion or extension. The motor would then apply assistance-as-needed to avoid the previously stated concerns about users allowing the motor to work for them. Many rehabilitative or assistive devices with more DOF use fuzzy control to decipher the patients intended motions. Fuzzy control differs from standard control techniques because it provides a formal methodology for implementing a human's heuristic knowledge about how to control a system. [28] More explicitly, a fuzzy controller is an artificial decision maker. It gathers data and uses comparison (typically through IF-ELSE statements) to "decide" what a plant input should be. A diagram of a fuzzy-control system with five inputs and one output can be seen below in Fig. 24. Each input is assessed by each rule and ultimately the best "decision" is made by the system and the appropriate output is delivered.

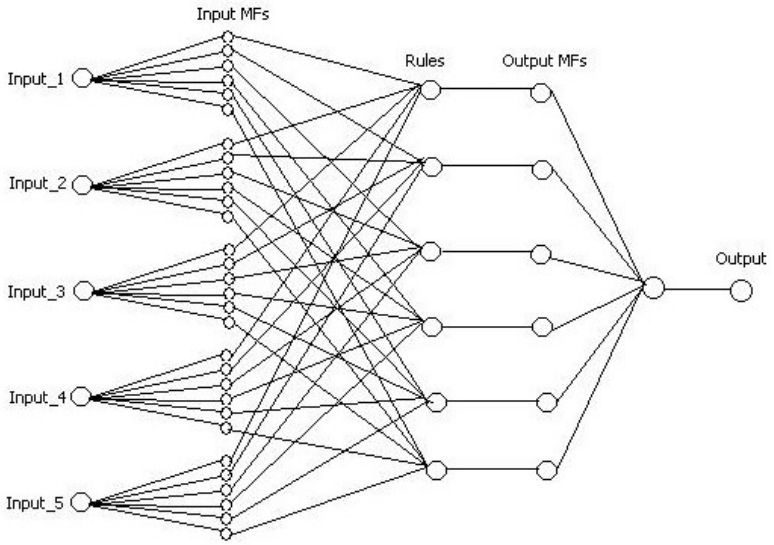

Figure 24: Example of a fuzzy control system [14]

For this project a quasi-fuzzy control system is introduced. Since there is only 1 DOF and the elbow joint can only flex or extend, there are not many decisions to be made. The quasi-fuzzy controller will take the inputs from each muscle, as well as both encoders, and decide what output to produce. The output from the system will simply be a current value calculated proportionally to the amount of torque necessary to either provide assistance- or resistance-as-needed. [19]

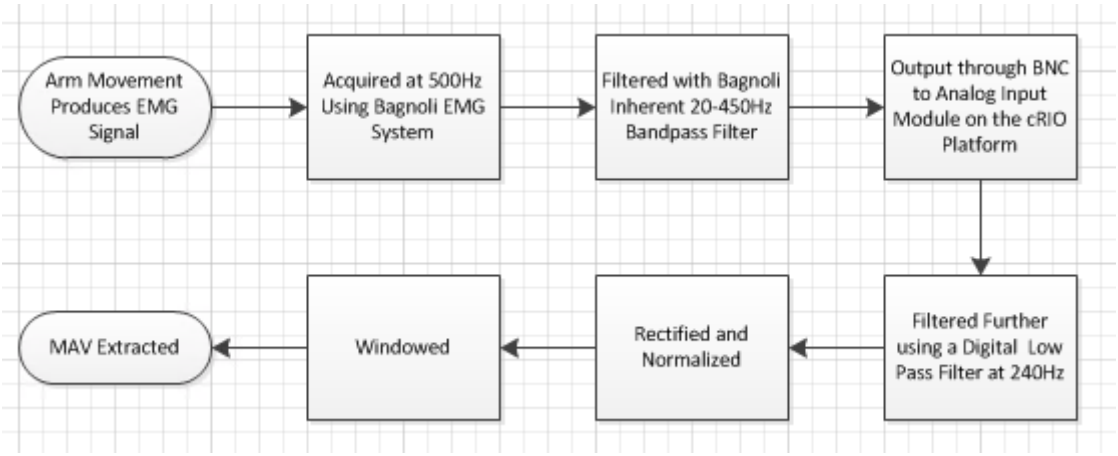

Figure 25: Flowchart of Myoelectric Control

Initially, the EMG data was extracted, filtered, and conditioned as previously mentioned. The MVC was determined by which the rest of the incoming data was normalized. Once the MVC was determined, a Boolean toggle switched the system to general data acquisition, displaying the filtered EMG signal. This data was split into window segments of 200 ms, which is less than the 300 ms required in order to eliminate delay. The MAV was calculated for each windowed segment and if the MAV crossed the threshold determined for that patient in that trial, the motor provided current inversely proportional to how far over the threshold the MAV was. Because this control modality was meant to guide bilateral motions, the motor also provided

current to the motor on the unaffected arm, where motion was resisted on this arm until the affected arm's threshold can be reached. This current is proportional to the amount over the threshold the EMG in the unaffected arm was. A resisting torque was provided if the MAV of the unaffected arm crossed its threshold while its encoder value was less than 200 ticks off from the encoder on the affected arm and if the patient had not reached the affected arm's threshold. The difference of 200 ticks corresponds to approximately 1% of the total stroke. This creates a situation where the patient cannot flex their unaffected arm until the EMG in their affected arm is large enough to cross threshold. With the thresholds easily controlled, the level can be increased over time as the patient increases strength and muscle activation.

2.5 Function Validation

Motion of the device was tracked in the Routine and Master-Slave control modes and subsequent analysis was performed using the data. Motion of the device was not tracked during Manual control because there were no unique results to be found. Motion of the device was not tracked using the Myoelectric control mode because this mode required a patient to wear the device and the scope of this thesis and prototype development did not involve gaining IRB approval to do patient testing. Instead, the EMG electrodes were worn outside of the device and the output of the system was tested to show motor activation when thresholds were crossed. Figure 26 shows the setup of the motion capture system in the Biodynamics Laboratory at the UConn Health Center

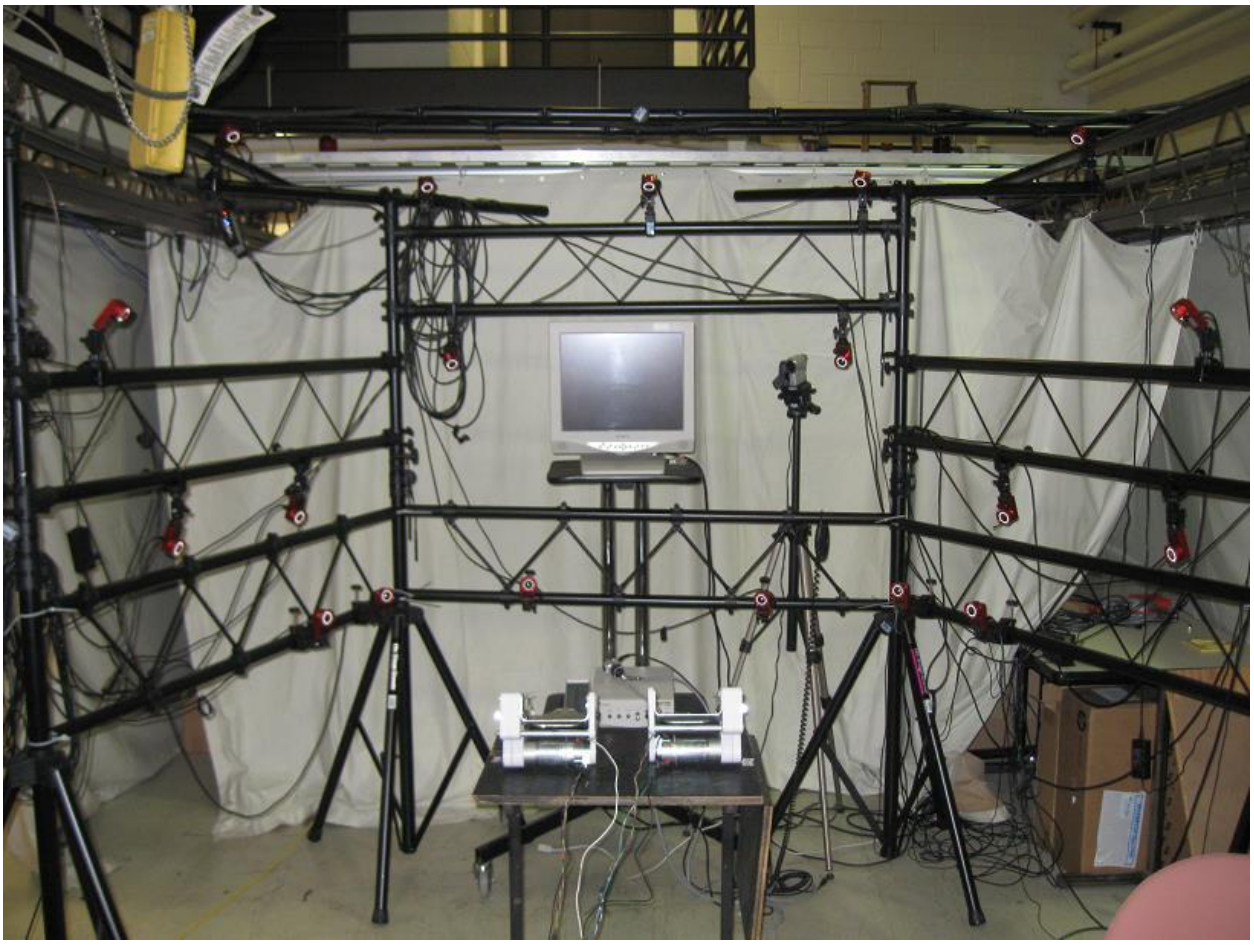

Figure 26: Motion capture setup

The OptiTrack motion capture system from NaturalPoint (Corvallis, OR) consisted of twenty-four cameras, where each camera emits infrared light and tracks the reflection of retro-reflective markers placed within its field of view. Each time the system is used, it needs to be calibrated, which consisted of several steps to make sure all the cameras were all in sync. Calibrating the system required two items: the calibration square and three marker wand seen on the left and right of Fig. 27, respectively.

Figure 27: Motion capture calibration square and three marker wand

First, the calibration square was placed within the collective viewing field of all the cameras. All twenty-four cameras needed to see all three markers on the calibration square. If all three markers could not be seen by any particular camera, that camera needed to be moved or adjusted in order to see the markers. Since each camera emits infrared light and many of the cameras are in the viewing field of other cameras, the cameras picked up each other as additional markers. To remedy this, the other cameras that were seen as markers by each camera were eliminated from the view by a function in the motion capture software used to "block all visible markers." At this point, the three-marker wand was spun continuously in the collective viewing field as each camera tracked it and collected data points. This process is referred to as wanding. These data points were then used in the software to synchronize each camera and to ultimately provide only one set of coordinate data per marker. Wanding is the most crucial part of the calibration process and poor wanding can lead to poor motion capture data and marker confusion by the system. Once the system was calibrated tracking could begin. It must be noted that the shiny aluminum arm frames of the device reflected the infrared light so white towels were

draped over the aluminum during motion capture. These towels were observed to not interfere with the function whatsoever.

2.5.1 Routine

For the Routine mode, the flexion and extension cycles were tracked and a sample of five cycles was taken to show the repetitiveness of the control mode. The left and right arm devices were tested individually to not only show the repetitiveness of each arm routine but to compare the data against each other. In addition, this tested if a patient would get the same treatment whether left or right arm was the affected am. There were three markers placed on each device: one at the upper arm, one at the elbow and one at the forearem. This marker configuration is shown in Fig. 28 below.

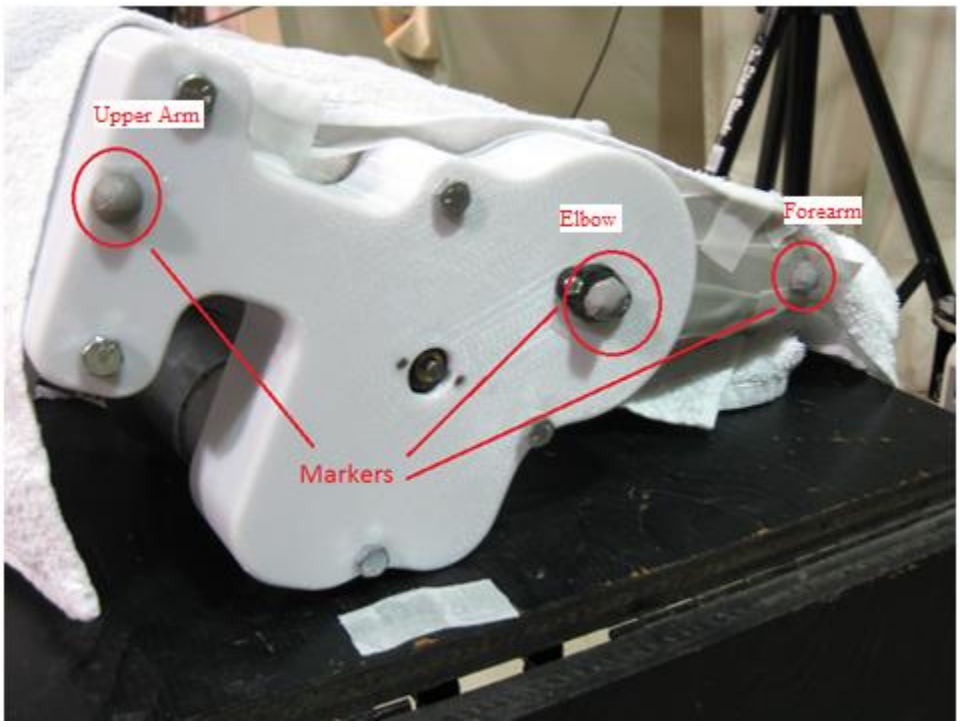

Figure 28: Marker Configuration

2.5.2 Master-Slave

The objective of the validation of the Master-Slave mode was to show that the device on the affected arm follows the unaffected arm instantaneously within the same range of motion. Data was captured while physically moving each arm's brace and controlling the other, in order to test indiscrimination between right and left affected patients. Furthermore, having data on either side, being both the master and slave, allows for the same type of comparisons against each other as the Routine mode. This bilateral data tested to see if the device would provide the same rehabilitation to left or right affected hemiparetic patients. The marker configuration remained the same as in the Routine testing validation.

2.5.3 Myoelectric

As stated, testing of the Myoelectric control mode could not be done with a patient, so EMG electrodes were worn outside of the device and the outputs were measured. The digital I/O module was set to output high when the motors were actuating and output low when the motors were at rest. The output from the digital I/O module was sent to a Tektronix TDS3034B oscilloscope along with the raw EMG data. This was done to test that, when the EMG is high enough to cross the threshold, the motors actuated.

3 Results

3.1 Mechanical Design

Only one of the finished devices is shown and it is understood that an exact mirror image exists. Figure 29 shows the full mechanical design after it was fabricated. The final device weighs 7.2 lbs and was just over 8 inches at its thickest width. At full extension, the brace

measured 17.25 inches from the midpoint of the top of the upper arm frame to the midpoint of the thin tip of the lower frame.

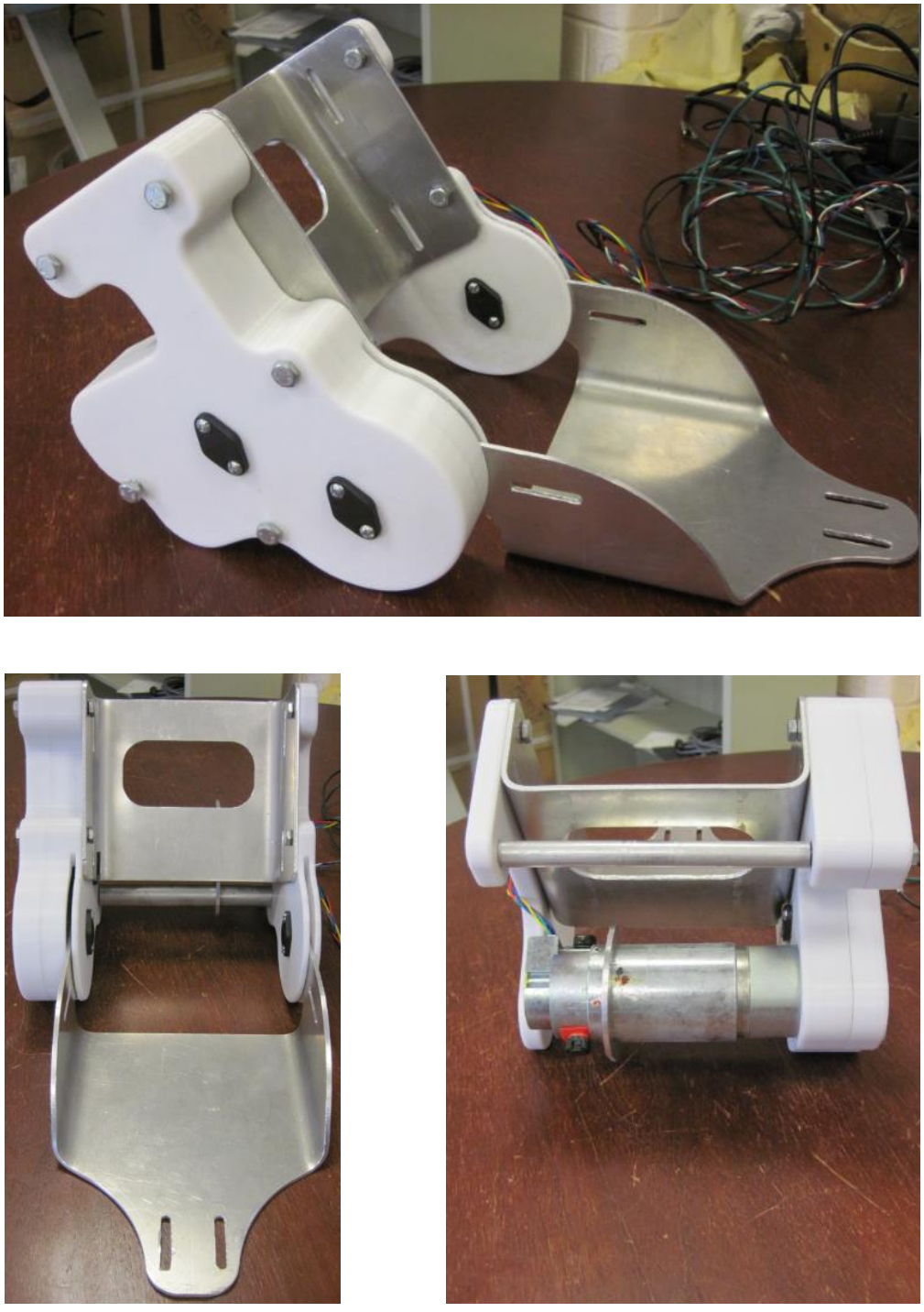

Figure 29: Completed mechanical design

3.1.1 FDM Rapid Prototyped Models

After the model was completed in SolidWorks, an STL file of each piece was generated. (STL files are used for rapid prototyping because they only describe the surface geometry of a three dimensional object. In the STL file format, the surface is described by any number of triangles, where more triangles generally represent a more complex surface.) The STL files were sent to Quickparts Inc. and were realized using the FDM process described earlier. The following image in Fig. 30 shows the Lateral Arm Support as an example of the details of the final "printed" pieces.

Figure 30: FDM model of the Lateral Arm Support

3.1.2 Arm Frames

The arm frames came out as expected with difficulty only arising in precisely bending the aluminum pieces so that the wings fit into their required slots in the FDM models. It was crucial

to bend the wings so that they move fluidly within these slots. Figure 31 shows the final bent aluminum pieces, with the slits cut for the Velcro straps. Three holes in a triangle arrangement can be seen on the near side wing of the arm frame. These were not originally planned and do not appear in the SolidWorks model. Throughout fabrication it was determined this would be the most efficient way to interface the frame with the rotating large pulley. The pulley has three holes in the same shape and the two are screwed together to transfer motion from the drive train to the arm frame.

Figure 31: Finalized Aluminum Arm Frames

3.1.3 Actuation

Due to the initial over estimatation, the selected motor provided the torque necessary, even with the lowered gear ratio. One full rotation of the spindle coincided with approximately 13,000 ticks of the encoder and the mechanical hard stops allowed for approximately 112°

degrees of flexion. Using the drive train ratios and the available degree of flexion, it was decided to use 20,000 ticks for full stroke motion to keep the arm frames slightly off of the hard stops. The motor weighs 2.85lbs, which was just under 40% of the total weight of the device.

3.1.4 Drive Train

Ultimately the motor spindle was fastened with a one-inch pulley. This pulley was connected via a timing belt to a two-inch pulley sitting on the intermediate shaft. This small pulley on the same shaft rotates in unison with the two-inch pulley from the first step. This second one-inch pulley is connected via timing belt to the three-inch pulley on the elbow axis of rotation. With a 2:1 and 3:1 ratio respectively, this drive train creates a 6:1 torque increase. Since the motor outputs a max continuous torque of 124 oz-in, it is possible to provide up to 744 oz-in of torque, if necessary. It is important to note that there was some trouble with belt slippage at high torques.

3.1.5 Safety

The only mechanical safety measure in the design here are the mechanical hard stops. To validate these safety stops, the motor was actuated with full load current, 5.91A as in order, to see the effect of the strongest possible torque on the integrity of the FDM materal. Once the arm frames reached the stops and the motor was still actuating, the timing belts began to slip and the FDM models maintained their integrity. Although this situation could potentially damage one of the pulleys or tear a timing belt, it is clear the patients arm has no chance of hyperextending.

3.2 Electromyography

3.2.1 Acquisition

The Delsys Bagnoli handheld EMG system provided exceptional EMG signals. The system's BNC output provided direct connection to the analog input module used in cRIO. The skin interface of the disposable adhesives provided a strong bond between the electrode and skin and the concavity between the parallel bars allowed for the skin to be pulled very tightly against the contact material. In addition, Delsys provided same patient reusable, yet ultimately disposable, self-adhering electrodes to acquire a reference signal. Figure 32 is a picture of the electrode placement used during testing, matching the SENIAM guidelines discussed previously.

Figure 32: Electrode placement for the bicep (left) and triceps (right)

The raw EMG acquired was of very high quality and a sample of the raw EMG data from the right bicep and triceps is shown in Fig. 32. Much like the typical EMG signal shown previously in Fig. 18, the muscle contractions are very clearly defined. This figure below shows four flexion-extension cycles using the Bagnoli system. The dark blue corresponds to the bicep

and the light blue corresponding to the triceps. It's clearly evident that the bicep is activated during flexion and the triceps is activated during extension.

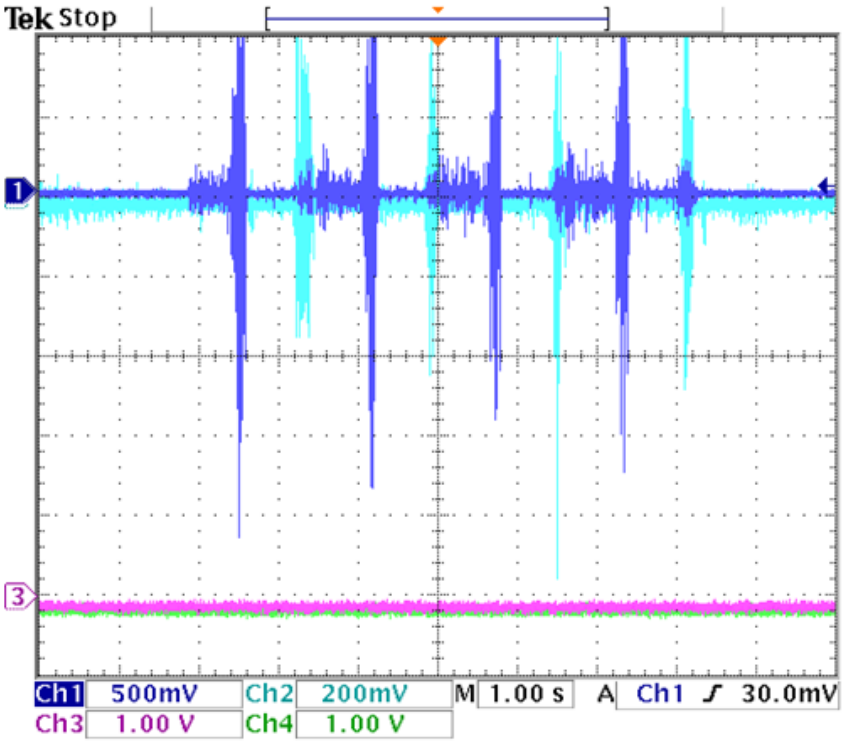

Figure 33: Raw EMG Signal acquired with Bagnoli system

3.2.2 Filtering and Amplification

Based on the reviews of similar work presented previously, a 500 Hz sampling rate was tested and proved sufficient for this application. Through experimentation, it was determined to amplify the signal by 1,000 using the built in amplification of the Bagnoli system. It was stated that the inherent bandwidth of the system was 20 to 450 Hz, but the high pass cut off was lowered to 240 Hz within LabVIEW in order to satisfy the Nyquist Criterion for a 500 Hz sampling rate, where the Nyquist Criterion states that the largest frequency component of a signal must be no more than half the sampling rate.

3.2.3 Conditioning

Through the development of this system, it became very clear that Eq. 1, the non-recursive equation for MAV, should be used. Furthermore, due to the limited amount of data to process in this application, the adjacent windowing technique was better suited to segment the data and eliminated the need to deal with redundant decisions. A window size of 100 samples was chosen and corresponds to 200 ms at the 500 Hz sampling rate, which is well below the 300ms maximum allowed for acceptable delay.

3.3 Control

The control modes all had proper interfaces on the front panel and provided the correct output. The coding was completed with parallel loops in the FPGA and a single loop in the RT, containing a case for each control mode.

3.3.1 Manual

LabVIEW offers only true-false Boolean toggles, so two were required for the control of each brace. Figure 34 shows the four states each pair of toggles could be conformed to.

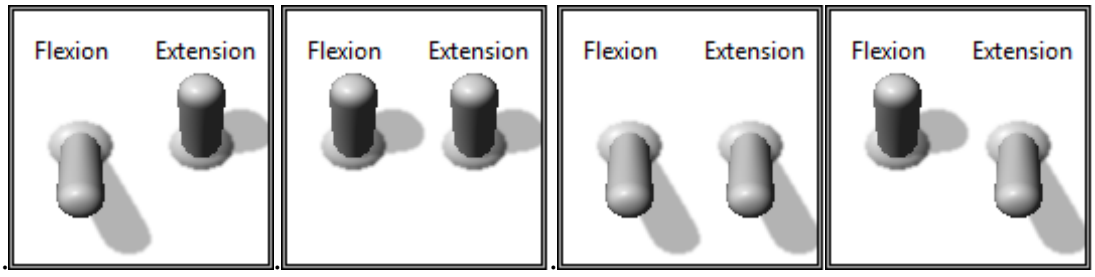

Figure 34: Possible conformations of Manual control toggles

The first is the neutral, or resting, state where nothing occurs. The second is for flexion and the third is for extension. The labels may look confusing at first, but it's clear to understand that if both toggles are "up" the elbow will flex, and if both toggles are "down," the elbow will extend. The fourth, which provides no meaningful output, disables the motor and stops the program if realized. The toggles would always be in the first conformation to start and the user would click a toggle to start either flexion or extension and then click that same toggle to stop motion before switching to the other.

3.3.2 Routine

This entire control modality was based around one LabVIEW function block, the RS Bistable, more commonly known as a flip-flop. This block simply accepts two Boolean conditions and "flip-flops" between "true" and "false" outputs as the conditions are alternately met. Figure 35 shows how this block was used and the routine is performed on either arm individually.

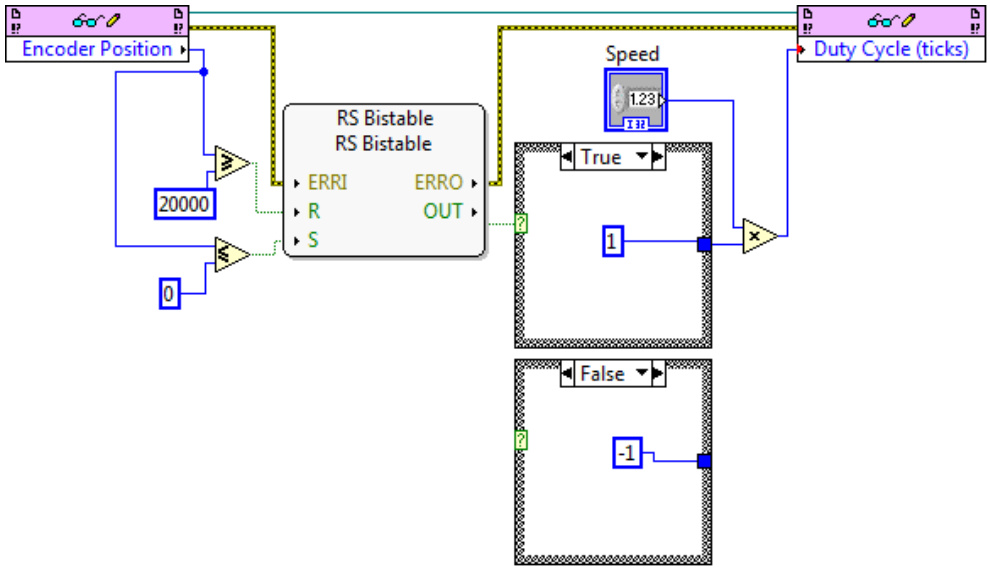

Figure 35: Use of RS Bistable for Routine control

The encoder output was read in the FPGA and extracted to the RT VI using the FPGA interface Read/Write block. This block is how data was passed between the two VI's in all cases. This value was then checked for both "less than or equal to 0" and "greater than or equal to 20000," which, as previously mentioned was the number of encoder counts used for full stroke flexion-extension. On the RS Bistable, the "R" and the "S" stand for "Reset" and "Set" respectively. The block first reads the "Set" condition and outputs true or false according to this condition. The output remains that way until the "Reset" condition is met, upon which the output is flipped. At this point the block goes back to monitoring the "Set" condition and the output returns to its original true or false value when it is met. The oscillation continues indefinitely, until the user stops the routine.

For this application and when the Routine mode starts, the encoder values are zero and the "Set" condition of less than or equal to zero is met. This provides a true output from the RS Bistable, signaling the true case and outputting a positive "1." This positive is multiplied by the desired speed and delivered back to the FPGA to be used in the duty cycle for the motor. At this point the output remains true so the motor spins in the positive direction until the encoder count reaches 20,000 and the "Reset" condition is met. When the reset condition signals, it flips the output to false, initiating the false case and outputting a negative "1." This is multiplied by the desired speed and motor spins in the negative direction until it reaches zero and the "Set" condition is met again, flipping the output back to true.

It is important to make the distinction that this function block does not output the answer from the condition to test; rather, it establishes a true or false output based on the initial "Set" condition and then flips that output appropriately as the oscillatory conditions are met. What this block does not do is check the "Set" condition and provide the correct Boolean output and then

check the “Reset” condition and provide that Boolean output. For instance, in this particular setup the initial “Set” condition is true and remains true until the “Reset” condition is met. It requires a *true* input from the “Reset” condition to make the output *false* (perhaps initially sounding counterintuitive).

3.3.3 Master-Slave

While the patient has both arms in their respective braces, he or she would flex and extend their unaffected arm, which back drove the motor and produces changing encoder values. The value of the other motor’s encoder was compared to this changing one and the motor on the affected arm’s device spins in whichever direction is necessary to follow along. The speed of the following motor could be adjusted to provide lag if desired but, for this application, it was presumably tested high enough for the symmetrical passive movement to be essentially instantaneous. In order to prevent the motor from oscillating around, a specific encoder value within a range of +/- 200 ticks was used. This introduces a possible error of up to 1%. It is important to note that the motor can never stop directly on a specific encoder value and, if a range is not defined, the motor shakes as it oscillates around an encoder value without ever exactly stopping on it.

3.3.4 Myoelectric

The Myoelectric activated assistive-resistive mode was by far the most complicated control mode. This modality incorporated filtering, conditioning, a quasi-fuzzy controller, and proportional torque control. The Myoelectric control mode begins with capturing the MVC of the biceps and triceps for both the affected and unaffected arms. Once the MVC had been determined, the user would flip the toggle switch on the front panel starting data acquisition and

the MAV would be displayed on the front panel. By observing the updating MAV data, the user would set an appropriate threshold for the patient to cross. When both the user and the patient are ready the user presses the "Begin Active Assist" button on the front panel. This button would only be pressed when both arms were in the fully extended position and both encoder values were reset to zero.

Once the "Begin Active Assist" button was pressed, the quasi-fuzzy controller would take command. Based on the MAV of muscles crossing threshold, as well as instantaneous encoder positions, the fuzzy controller would decide when to provide assistive or resistive torque to the affected or unaffected arms, respectively. The output of the fuzzy controller is simply two current values in amps, one for each motor. These current values range from zero to the user-controlled Current Limit on front panel and are either proportional or inversely proportional to the amount over threshold that was reached.

3.4 Validation

For the two modes validated using motion capture, both the upper arm and elbow markers remained stationary; therefore, the forearm marker moving with the flexion and extension of the lower arm frame was the marker of interest. The coordinate system was set for the xz-plane to be the floor and the y-axis to be vertically upwards. Although the marker moved in an arc, the braces were set so flexion was always in the positive y-direction. Since there was no change in the y-direction of marker movement for either a flex or extend stroke, the y-axis data was sufficient to characterize the full range of motion.

In addition to this, it was important to look at the angle of elbow flexion, in order to characterize the degree of motion available from the device. It was also important to look at

movement in the x-direction to determine lateral shift during flexion or extension. Rather than providing similar data for both arms in all control methods, these tracked motions are presented here for the right brace in the Routine mode. First, since the upper arm and elbow markers remained stationary, the coordinate system with the respect to the motion capture calibration was translated to the upper arm marker of the brace. It was important to see if the translated coordinate system was uniform throughout the stroke, so the xyz coordinates of the upper arm marker was plotted with respect to the first point in the data for a five cycle sample. This graph is shown in Fig. 36 below. The figure shows that the movement of the marker was greatest in the z-axis with only about 2 mm as the maximum. In addition, the error was observed consistent throughout the five cycles.

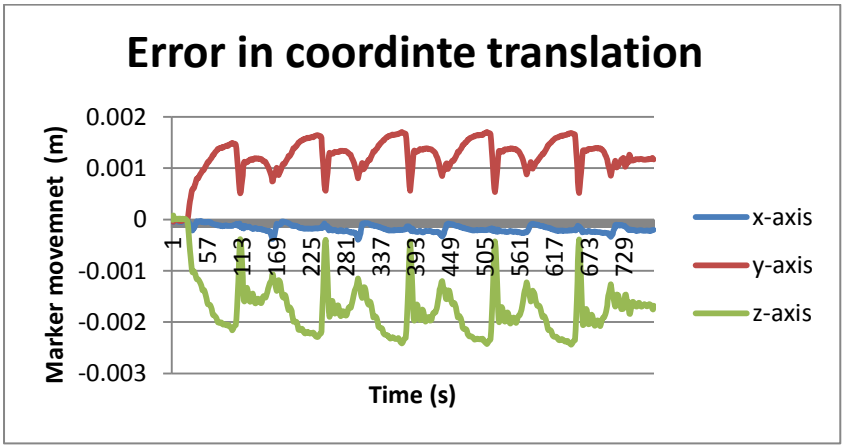

Figure 36: Error of coordinate translation with respect to the first point of data

The characterization of the movement in the x-axis of the right forearm marker for the same five cycles, which corresponds to lateral shift in the brace as it performed vertical flexion and extension, is shown in Fig. 37. This figure shows the largest shift was approximately 15 mm and was observed to be consistent during each cycle. Since the shift is consistent and does not affect the flexion and extension movements, the projections of the markers onto the yz-plane

were used to characterize the angle between the stationary upper arm-elbow vector ($\overrightarrow{UE}$) and the moving elbow-forearm vector ($\overrightarrow{EF}$).

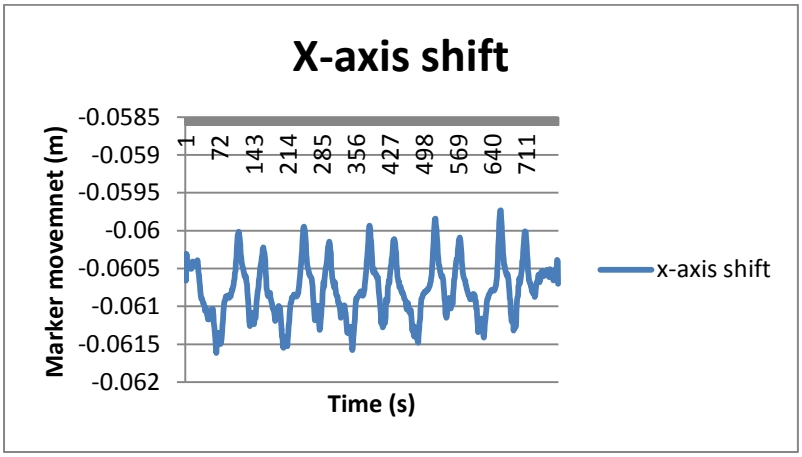

Figure 37: X-axis shift during right brace Routine

Characterizing elbow flexion was done by plotting the maximum flexion and maximum extension, then using vector algebra to find the angle between. In the plots shown below in Fig. 38, the three markers are displayed in white, the stationary vector between the upper arm and elbow markers is in blue and the moving vector between elbow and forearm is in red.

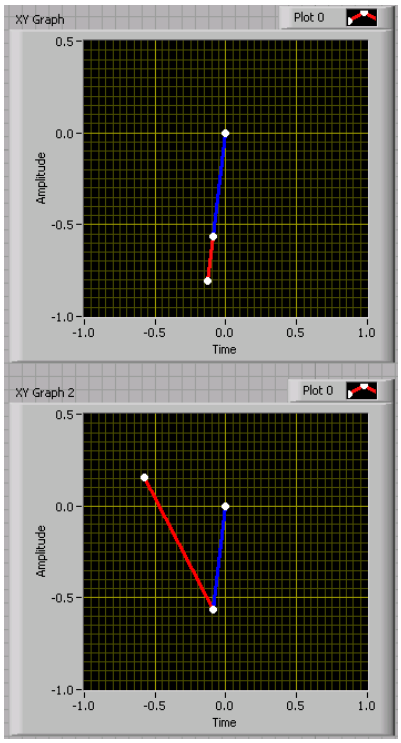

Figure 38: Plots of marker configuration during full extension and full flexion

The upper plot shows the device in full extension and the lower plot shows the device in full flexion. Using Equation 3, the angle between the two vectors was found, where the operation in the numerator corresponds to the vector dot product. Using Equation 3, the angle was determined to be 121° for full stroke motion.

$$\theta = \cos^{-1}\left(\frac{\overrightarrow{SE}\cdot\overrightarrow{EW}}{\|\overrightarrow{SE}\|\|\overrightarrow{EW}\|}\right) \qquad \text{Eq.3}$$

These errors and ranges of motion were similar throughout all control modes and are illustrated before introducing each control mode in order to avoid redundancy in the thesis. However, motion capture data is also analyzed for function in the Routine and Master-Slave modes.

3.4.1 Routine

For the Routine mode, the devices simply oscillated flexion-extension cycles and motion capture reflected this with numerical support. Figure 39 shows the y-axis value of both the left and right forearm markers as they gave a five cycle sample. For the left brace, neglecting the initial delay between camera initiation and the start of actuation, the sample took 12.12 seconds, averaging 2.42 seconds per cycle. Neglecting the short initial period for the right brace, the same speed produced a 13.70 second sample for the five cycles, resulting in 2.74 seconds per cycle.

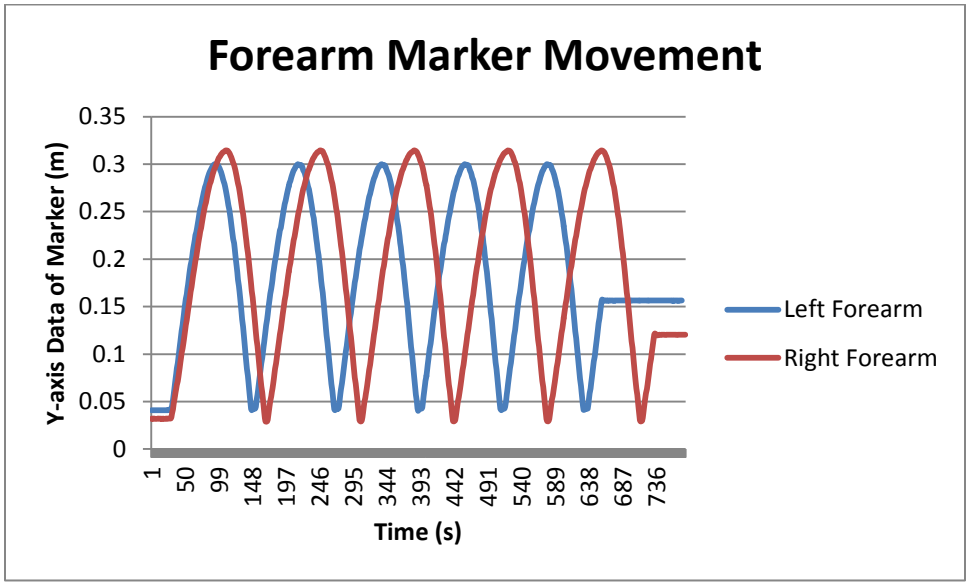

Figure 39: Y-axis data of the left and right forearm markers during respective routines

Taking the minimum values between cycles, the standard deviation of the left brace data is .022 s while the right is .032 s. Although the standard deviation on the right is slightly larger, both are quite small compared to the data. This means the individual cycles for both braces are characteristic of their average and no cycle was observed to skew the average data. Table 2 below illustrates the times per cycle as well as mean and standard deviation of the Routine

validation. Under no load, it is clear to see that, at the same speed, the right brace was consistently three-tenths, or 13%, longer per cycle than the left.

Table 2– Cycle data for Routine mode, all values in seconds

	Left Forearm Marker	Right Forearm Marker
Cycle 1	2.46	2.78
Cycle 2	2.42	2.76
Cycle 3	2.42	2.70
Cycle 4	2.42	2.72
Cycle 5	2.40	2.74
Mean	2.42	2.74
Standard Deviation	0.22	.032

3.4.2 Master-Slave

As this mode was controlled at the will of the patient, it was not so much concerned with timing as with synchronized motions. It does not matter how long each cycle took because the patient would be flexing and extending their unaffected arm at whatever speed they chose. Figure 40 shows three cycles for each arm acting as the master. For both of these graphs, the red line denotes the right forearm marker's movement and the blue line denotes the left forearm marker's movement. For both graphs, the data for the slave (affected arm) is placed on top. Ideally these lines would be directly overlapping one another.

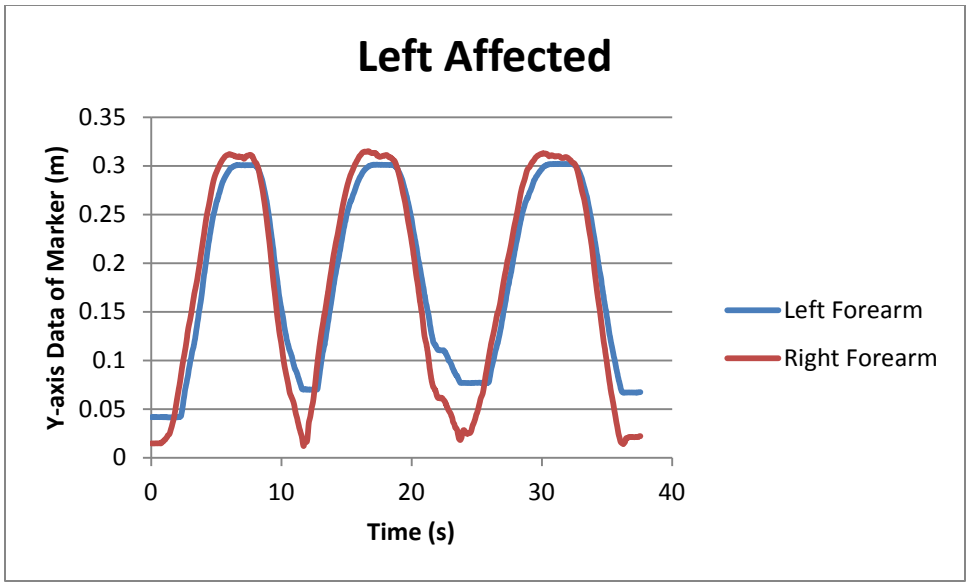

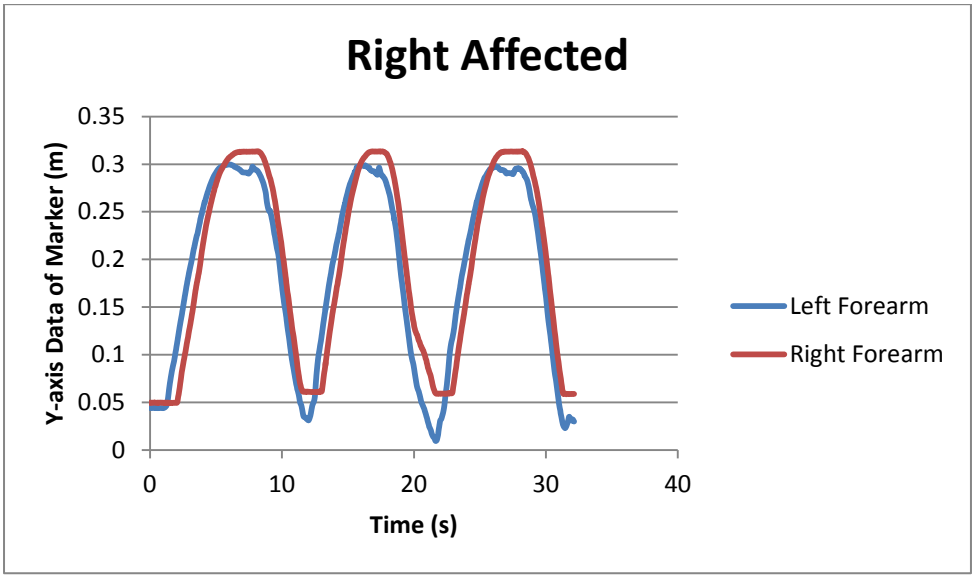

Figure 40: Y-axis data of both left and right markers for both Master-Slave scenarios

By visual inspection, it is clear that, in both cases, the slave could not follow the master to the bottom of its stroke. Also, the there is a slight delay between the master and slave in both the flexion and extension directions. Despite these, the slave did follow the general trajectory with the largest deviation occurring at changes of direction. For the left affected arm scenario, the largest difference in y-axis location was 0.059 m, at the 23.72 s mark. This was just slightly

larger than the previous cycle, where a difference of 0.059 m at the 11.70 s mark was seen. In the right affected arm scenario, the largest difference was 0.050 m at the 21.65 s mark followed by 0.036 m at the 31.45 s mark very close to the end of the sample.

3.4.3 Myoelectric

The most important thing to demonstrate was to show that, when a threshold was crossed, the motors actuated. More specifically, that both braces worked together to assist or resist torque, when the respective muscles crossed threshold. The following set of images is where the digital I/O module on the cRIO was used. Both the Bagnoli EMG systems and a pair digital out pins from the cRIO were hooked up to the same oscilloscope. For all of the following images, the dark blue EMG signal comes from the "affected" arm (left bicep) and is paired with the purple digital out line. The light blue EMG signal comes from the "unaffected" arm (right bicep) and corresponds to the green digital out line. Figure 41 shows the system at complete rest.

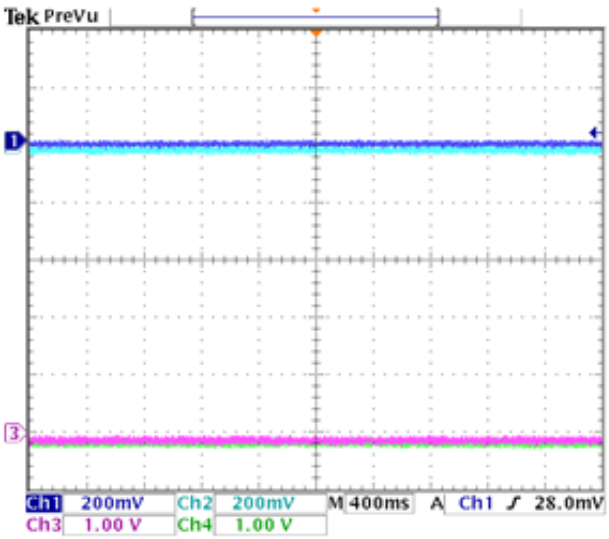

Figure 41: Resting state during Myoelectric control

During activation, the raw EMG data is equally positive and negative about their resting baseline. The purple and green lines are at digital low and jump up just over three divisions when their corresponding motor actuates. Figure 42 below illustrates how the system looked when the left bicep crossed threshold to actuate the motor, then loses threshold as well as motor assistance, then crosses again to receive additional assistance. It is clear that the system delivered correct outputs but with a slight delay.

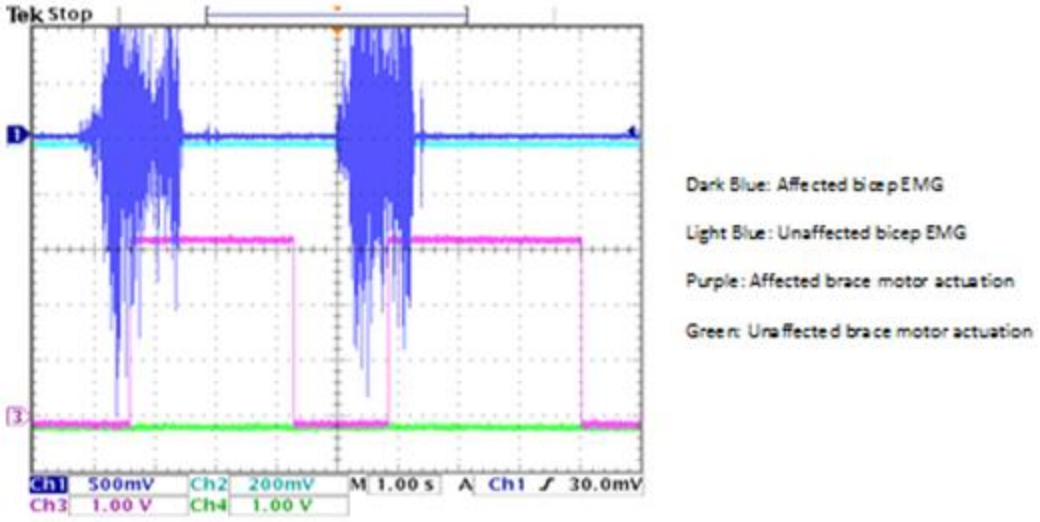

Figure 42: Motor activation from crossing bicep threshold

Finally, it was necessary to show that the system can produce simultaneous assistance and resistance if needed. In addition, the resistance of the unaffected arm should only be provided while that arm has crossed threshold. Figure 43 gives an illustration of this scenario. Right away both arms crossed threshold, so both digital out lines went high. Then, the right unaffected arm lost threshold and this arm's motor stopped actuating. The left affected arm continued to hold threshold and the assistance was observed to continue until the threshold was lost. Again, it is clear that the system delivered the correct outputs but with a slight delay.

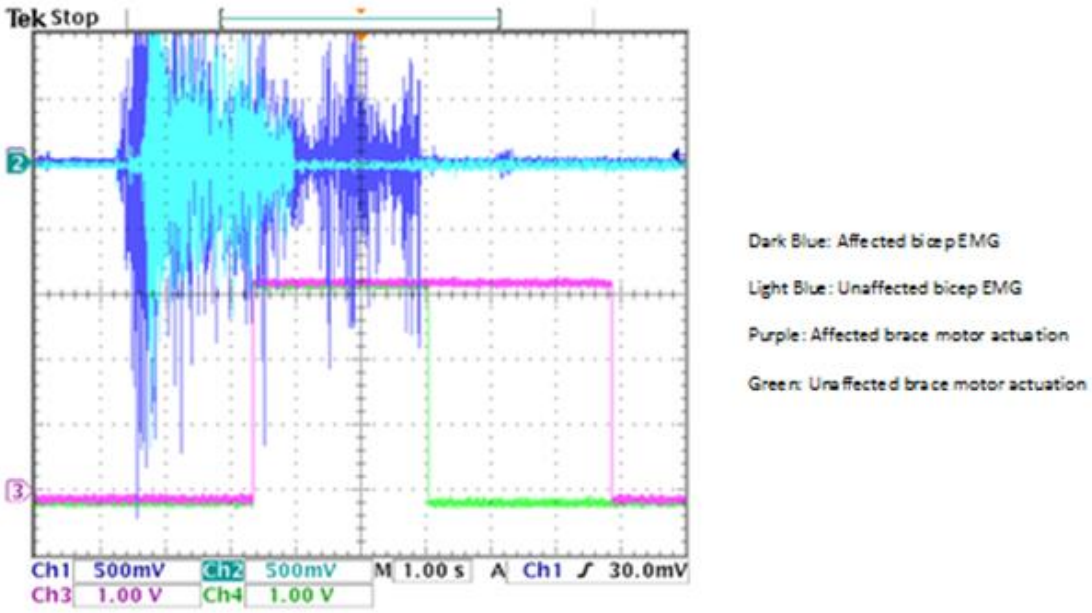

Figure 43: Simultaneous activation of assistance and resistance

4.0 Mass Production

If this device is to move on to mass production, the components will certainly not be 3D printed but most likely injection molded. Injection molding is the ideal process of producing high volumes of plastic parts because it has high tolerance precision, repeatability, minimal scrap losses and a large material selection. [31] In general, after a mold of the desired part is complete, granular plastic is melted down and forced through a nozzle into the mold cavity. The mold remains at a set temperature so that the plastic can uniformly solidify as the mold is filled. [31]

4.1 Part Redesign

In order for these pieces to be successfully injection molded, they needed to be redesigned to fit certain specifications for the process. Most importantly, the pieces needed to have uniform thickness so that the material would cool evenly. Rather than describing each

piece, only the Lateral Arm Support will be detailed and it is understood the other pieces were treated similarly. Figure 44 shows the design for the two pieces side by side.

Figure 44: Comparison between designs for 3D printing (left) and injection molding (right)

It´s clear that the piece designed for injection molding uses much less material and has a uniform thickness ideal this process. Consequently though, it´s apparent this piece will have less strength and may not be able to endure the torques that the original 3D printed piece could. It is obvious that injection molding these pieces would be worthless if they were too weak to function properly, so stress analysis was performed on both the original 3D print designs and the new injection mold designs to compare. Before meaningful stress analysis could be performed on the injection mold designs, their feasibility to be injection molded needed to be proven first.

4.2 Simulation Moldflow

Feasability of injection molding was done using the program Simulation Moldflow. Simulation Moldflow is engineering software owned my Autodesk Inc. (San Rafael, California,

USA) which provides simulation tools for injection mold design. First, the new designs specific for injection molding were tested. An injection site was automatically chosen by the program as to coordinate having the mold reach its furthest point in all destinations as close to the same time as possible. Figure 45 shows the filling of the model over time, with the inverted yellow cone representing the injection site.

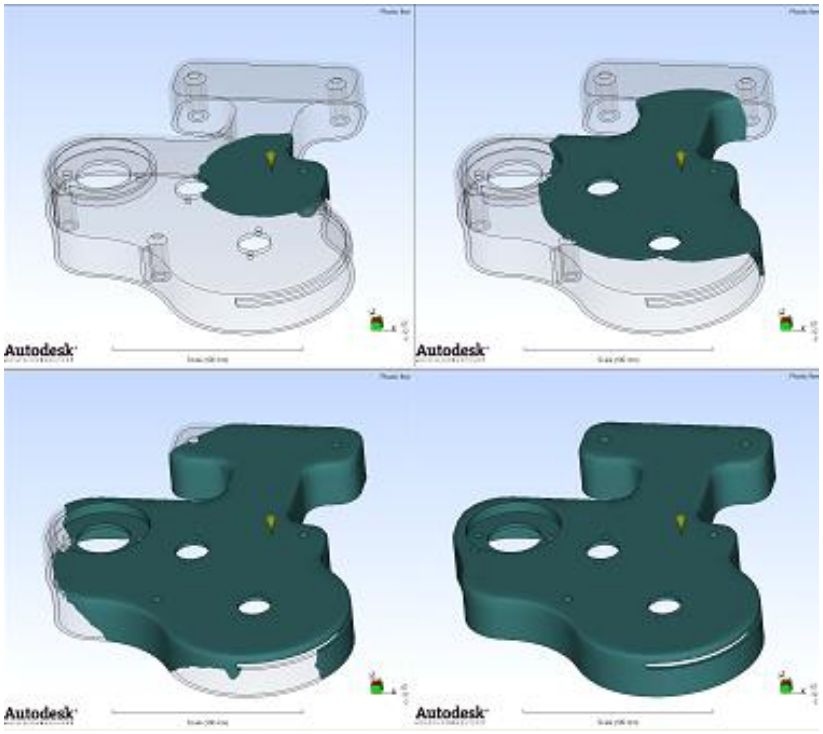

Figure 45: Injection mold filling over time with optimal injection site

More important than the visual time lapse of the mold filling are the actually results of the simulation. Four items were looked at in discerning the feasibility and quality of the design. First were Sink Marks, which are places around the edges where the mold might not fill properly and there could be variation in the material thickness. Second, the Cooling Quality was observed to determine if any problems would occur after the injection had finished. Third, the Confidence of Fill was a measure to see if the plastic could in fact reach within all of the parts of the model.

Finally, the Quality Prediction showed an estimate of how final piece will turn out. Figure 46 illustrates all four of these.

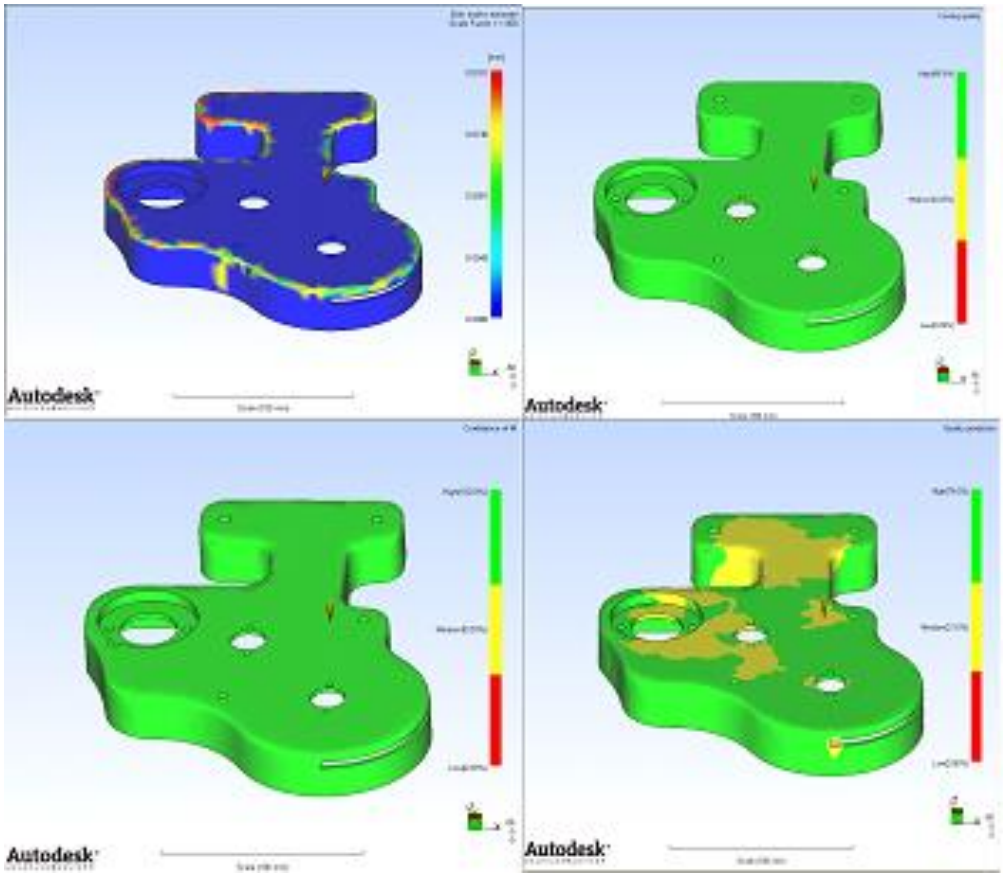

Figure 46: Sink Marks (top left), Cooling Quality (top right), Confidence of Fill (bottom left), Quality Prediction (bottom right)

From Fig. 46 it shows that the largest Sink Mark is 0.0181 millimeters, which is negligible for this application. The figure also shows an extremely high cooling quality (99.9%) and Confidence of Fill (100%). The Quality Prediction might seem like it could be unacceptable because the value of 79% high quality is a smaller number than the previous two. In fact, this is still very acceptable for this application because the vast majority is considered high and exactly zero-percent is considered low.

To test the optimality of the injection site, a suboptimal spot was chosen and the simulation was run again. Figure 47 shows the mold filling from the suboptimal injection site again depicted by the inverted yellow cone.

Figure 47: Injection mold filling over time with suboptimal injection site

For this suboptimal injection site three of the four criteria were almost identical, the Sink Marks, Cooling Quality and Confidence of Fill. The difference was in the Quality Prediction, where using a suboptimal injection site gave a lower ratio of high to medium quality, with 68% high compared to 79% for the optimal site. Similarly though, there was exactly zero-percent low quality areas. Figure 48 below shows the Quality Prediction for the sub-optimal injection site.

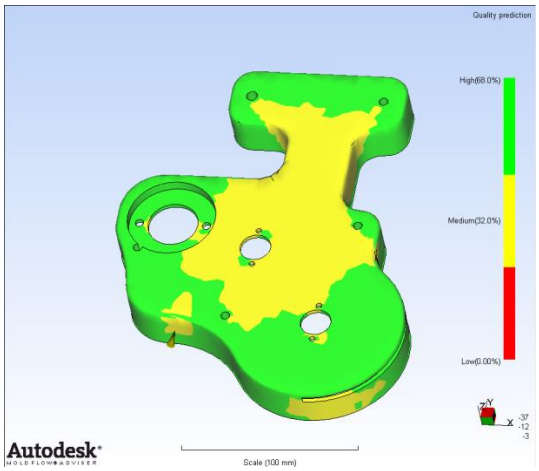

Figure 48: Quality Prediction for a sub-optimal injection site

Finally, the original 3D print designs were tested to compare the feasibility of injection molding these as opposed to the new designs with uniform thickness. For this case the optimal injection site calculated by the program was used. The results were quite similar, even negligible to that of the new designs in terms of Sink Marks, Confidence of Fill, and Quality Prediction. The major difference here was the Cooling Quality. Figure 49 below shows the Cooling Quality for the original 3D print design. Cooling Quality was found to be 12.1% low, mostly in areas with a lower thickness.

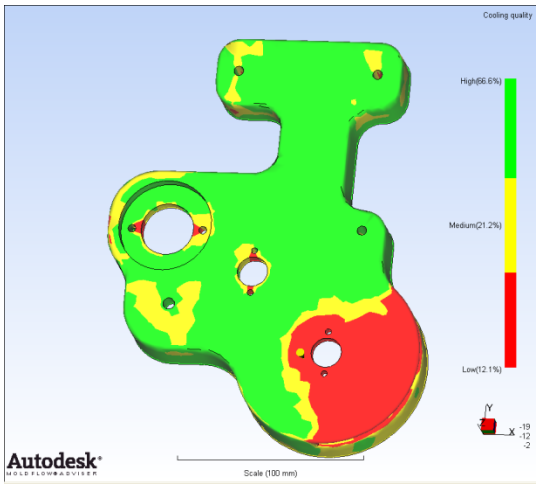

Figure 49: Cooling Quality for original 3D print design

4.3 Diagnostic Testing

The stress and deformation analysis was done using Siemens (Munich, Germany) NX 8.5. This program accepted the SolidWorks files directly and performed finite element analysis. Upon importing the files there were four steps to take in order to perform the analysis. First, it was important to apply a mesh to the part. Applying a mesh is essentially dividing the part up into many small pieces which individually react and deform to a given load. The size of the mesh elements must be smaller than the minimum thickness of the piece or else the result will be

inaccurate. Next, a material must be selected and applied to the part in order for the deformation to be consistent with a prototyped device. For the 3D print design, Polycarbonate was selected because that is what was chosen for the actual pieces. For the injection mold design, ABS was selected because of its mechanical properties and ubiquity within the industry. Upon meshing and choosing a material, the final two steps were to apply constraints and loads. The constraints, in both cases, were chosen as type ¨fixed¨ and selected as the holes where the screws go to hold the pieces together. The load was selected as a torque and applied where the motor is mounted to the device. This value used for this torque is the maximum stall torque of the motor used in the device. This value is 975 oz-in. Figure 50 shows the meshing, constraints and load on the design. The material selection, of course, is just stored in the program and cannot be seen.

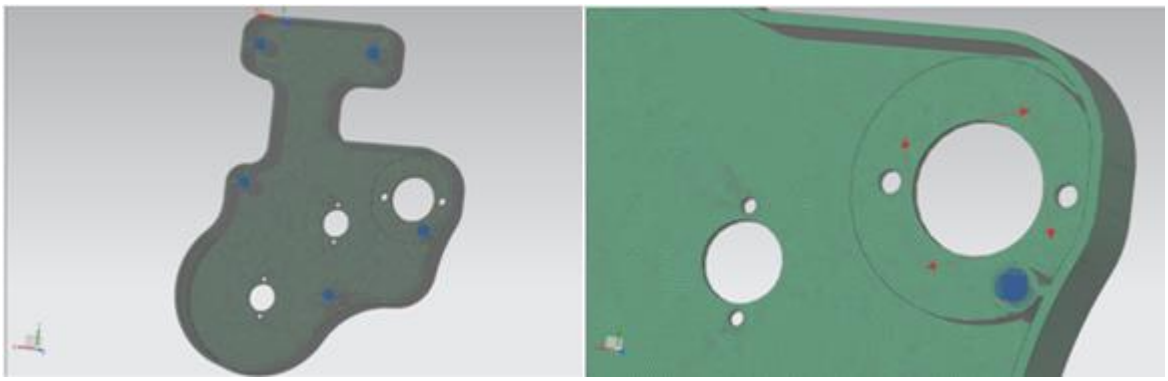

Figure 50: Meshing, Constraints and Applied loads using the injection mold design as an example

4.4 Diagnostic Testing Results

Once these four parameters had been set the system readily solved for both stresses and displacement. This procedure was first conducted on the original 3D printed design to gain a baseline of what was already prototyped. Figure 51 shows the stresses on the 3D printed part for the stall torque of the motor, 975 oz-in as mentioned.

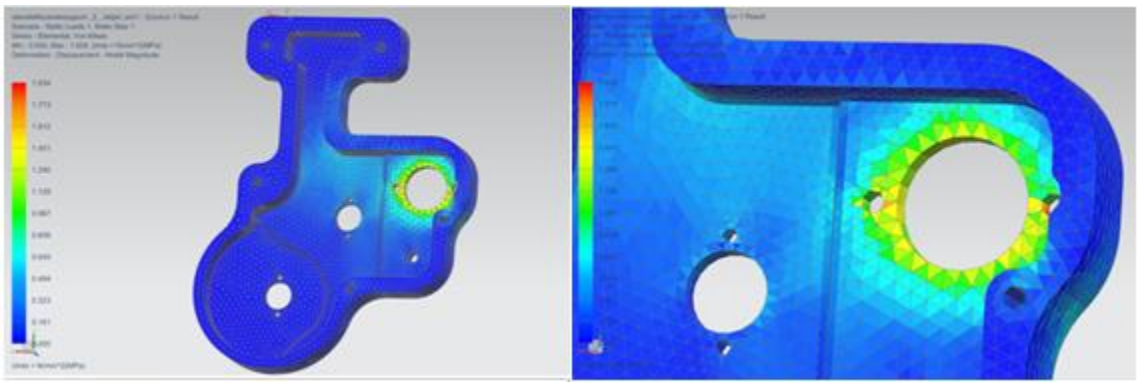

Figure 51: Stresses on the material during peak loading for the 3D print design

The stresses seen here are very low, with the peak being 1.934 MPa. This corresponds to approximately 280.5 psi. The displacement of the material is illustrated in Fig. 52 below; the maximum displacement is 0.0426 mm.

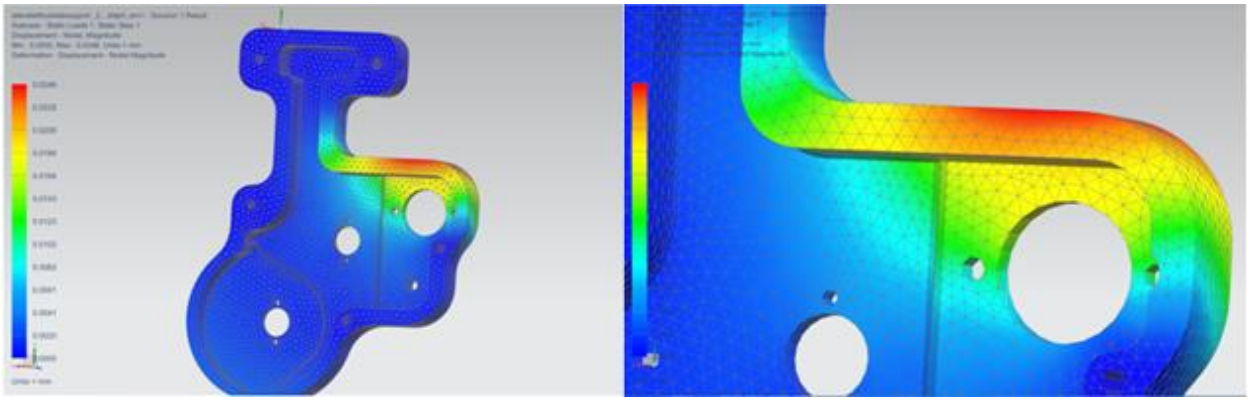

Figure 52: Displacement of material during peak loading for 3D printed design

After testing the 3D print designs, the injection mold designs were subjected to the same loading conditions to compare. Figure 53 below shows the stress distribution of the injection mold design for the same loading conditions of 975 oz-in of torque. The maximum stress value is 7.145 MPa which corresponds to approximately 1036.29 psi.

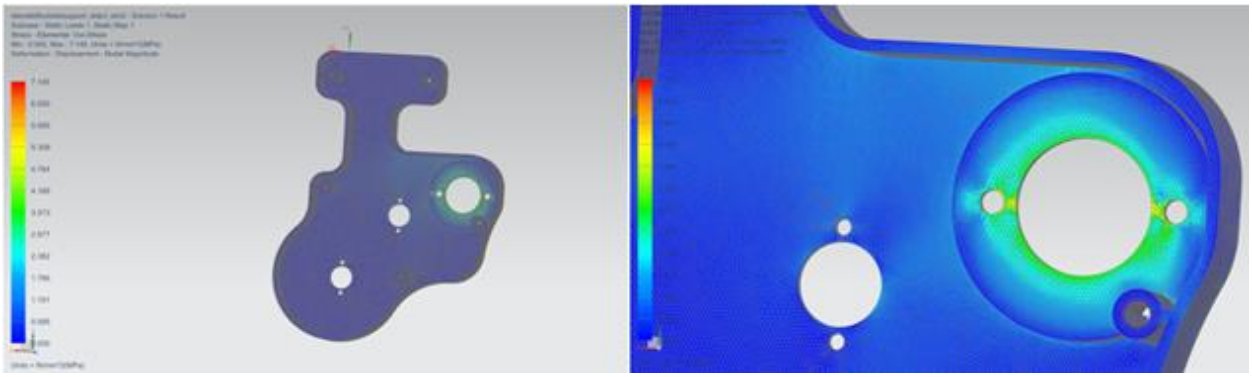

Figure 53: Stresses on the material during peak loading for the injection mold design

Similarly to the 3D print case, the displacement was also observed for the injection mold design. Figure 54 shows the displacement of the part when subject to peak loading. The largest displacement on the injection mold design is seen to be 0.136 millimeters.

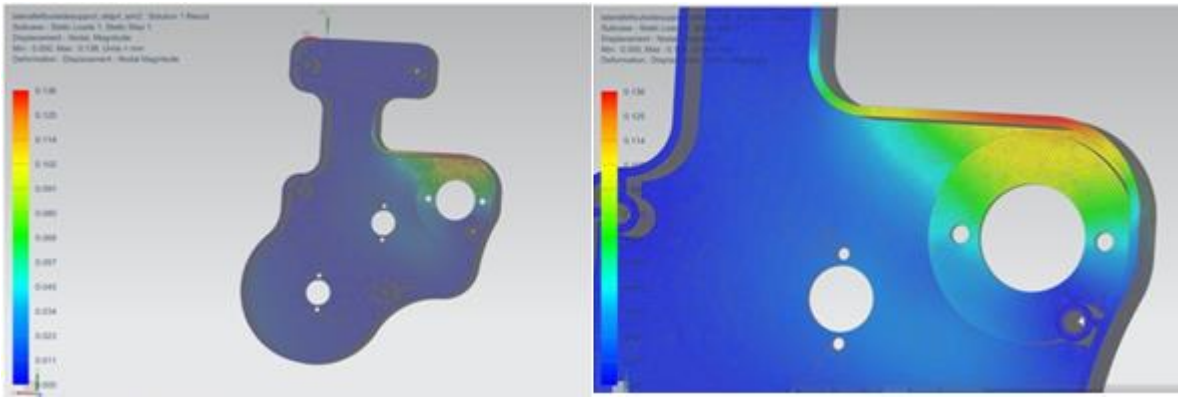

Figure 54: Displacement of material during peak loading for 3D printed design

It must be made clear that these simulations were done on the individual parts, when in reality there are two pieces held together which support the motor, the Lateral Arm Support and its cover. Testing the parts individually was in fact adding safety, because the two pieces together will be stronger. To prove this the simulation was run again on the injection mold

design, this time with the Lateral Arm Support and its cover joined together. The results are shown below in Fig. 55.

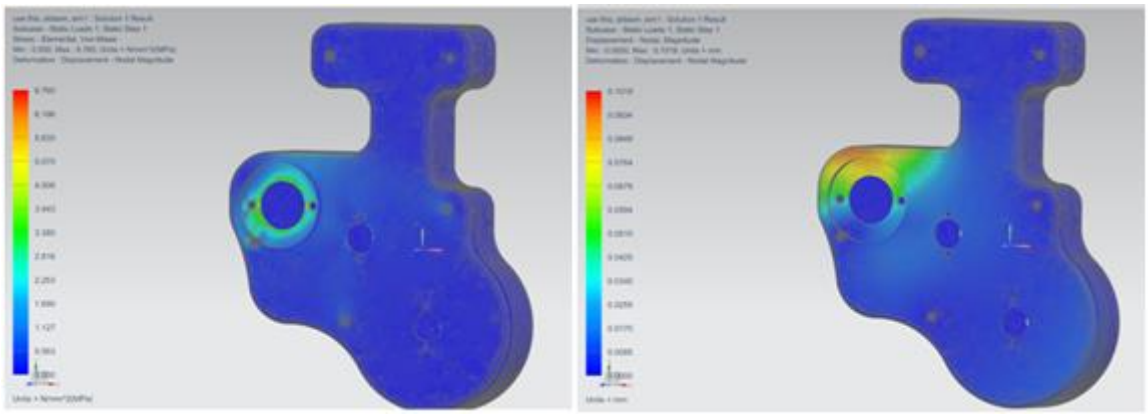

Figure 55: Stress (left) and Displacement (right) of the joined parts during peak loading for the injection mold design

The stress distribution is shown in the top picture, with peak stress at 6.760 MPa, corresponds to 980.46 psi. The bottom picture shows the displacement of the material with a maximum displacement of 0.1019 mm.

5 Discussion

The cRIO platform proved to be ideal for this project and the inherent re-configurability of the FPGA will suit the continuing research exceptionally. The ability to physically restructure the FPGA hardware to suit specific needs allowed for many potential ideas to be tested quickly, without having to acquire additional equipment. The communication between the FPGA and the RT module was very efficient and there was no apparent loss of data. Both the Analog Input and Motor Control modules worked flawlessly as well. The built in encoder feedback on the Motor Control module was one of the most critical pieces of this system. Having this inherent feedback, rather than using a potentiometer, saved the necessity for an additional Analog Input module.

Furthermore, it provided much more accurate encoder feedback over a noisy analog potentiometer.

The mechanical design came together very well with some small issues arising throughout the assembly process. The most apparent problem with the design is the size and weight, but this was expected with the first prototype. The issues that arose were mostly related to fitting and aligning all the pieces, which required some additional unexpected machining. The FDM supports came out flawless for the proposed design and could be redesigned to be smaller, lighter and more compact. Also, the degree of allowable flexion could potentially be increased. It must be noted that it was originally planned to machine these pieces out of aluminum but the FDM option was chosen instead for a number of reasons. Machining time versus the level of allowable complexity was the most important factor followed closely by the desire for a non-metal material. Furthermore, if the pieces were to be hand machined from aluminum, the time it would take to include all of the details would not be worth the complexity of the design. Simplifying the design and losing functionality would be required in order to manufacture the support pieces from aluminum within the desired time period. Lastly, it was originally hoped to use ULTEM over Polycarbonate for its superior mechanical properties but, unfortunately, this material was too expensive.

The aluminum arm frames caused most of the aligning problems because they were bent using a pipe on a hydraulic press to create a smooth radius. The pipe used for bending was not connected to the press and was placed by eye on a scribed line on the flat aluminum. The lack of proper machines indirectly caused these alignment problems. Once bent by the press, the wings were slightly bent back or forth to achieve fluid motion within the required slots in the FDM models.

The amount of actuation necessary caused a dilemma as well. The motors were the heaviest items on the braces and provided much more torque than necessary to assist in arm movement. The dilemma arose with the amount of torque necessary to resist arm flexion of the unaffected arm in strong patients. For three out of four control modes, a much lighter and less powerful motor would suffice but, in order to truly resist unaffected arm flexion in a strong male patient, a larger sized motor was necessary. The pulley and timing belt drive train further increased this torque by a six to one ratio, meaning that, if this was increased further, the size of the motor could be reduced. The drive train was originally planned to increase the torque by an eleven to one ratio but it proved too difficult to back drive the motor for the Master-Slave control mode. It is also clear that a new motor must be selected in order to greatly reduce the weight of the system. The pulley and timing belts worked for this application because they were the perfect size. In any future design, it would be imperative to incorporate some sort of slits for bearing mounting rather than just fixed holes. With slits, it would be very straightforward to mount a slacked belt and then pull it tight once the bearing had been loosely screwed into place.

The EMG signals acquired using the Delsys systems were excellent. Before these were purchased, a standard disposable Silver/Silver Chloride (Ag/AgCl) electrode was used. Although these may have provided a sufficient signal to complete the project, the quality of the signal was nowhere near that of the Delsys system. It's clear this signal quality is directly related to the built in features of the Bagnoli including, but not limited to, the built in filtering and amplification, the 99% pure silver connection, and the concavity of the reusable electrode to pull the skin onto the sensing elements.

Using MAV as feature characteristic provided a very straightforward way to characterize the patients muscle output. MAV is simply just the average muscle activation for a particular

amount of time (in this case, 200ms). This feature characteristic is a simple, yet powerful input into the fuzzy controller to determine how to actuate the devices. The non-recursive MAV equation was chosen because the system takes a segment, calculates the MAV, then produces an output based on the relationship between the MAV and the set threshold. It then takes the next segment and performs the same calculations. The segments are different but all the same size, so there is no need to calculate a recursive MAV, since the segment length is not increasing. Furthermore, the adjacent windowing technique proved superior for this application because the amount of data does not strain processor capabilities and the technique eliminates the need to account for semi-redundant decisions.

Although the Myoelectric control mode was the main focus during the inception of this project, it was acknowledged early on that expanding the functionality of the device was imperative. It was originally proposed to add just the additional Master-Slave mode and work began to complete a system that functioned with these two modalities. During the literature research, it was found that, in traditional physical therapy, a patient's hemiparetic arm was simply flexed and extended by a therapist for many repetitive cycles. The proposed system already planned to function with much more complexity than this and this flexion-extension Routine quickly became the third modality. As this project was being outlined, only complex control modalities seemed important to plan and discuss. Once testing of the code began, it quickly became apparent that having manual control would not only assist in design and testing, but also in practice. Each of the three other control modes were dependent on some sort of indirect control, never really giving the user direct control over a patient the way a traditional PT would have.

The Myoelectric control mode proved much more difficult to design than had been originally expected. The idea seemed straightforward and, with the NI Motor Control Modules boasting optimized current-torque control, most of any difficulty was expected to show up in using proper syntax within the graphical programming environment. Although this did cause some problems, designing control loops to function in sync was the biggest problem encountered. Timing and synchronization of data flow between parallel loops became almost impossible, since the code had to be augmented repetitively to account for the control modes being added one by one. Additionally, muscle fatigue caused issues during testing. After an extended period of activation, EMG signals weaken and the thresholds needed to be lowered to continue testing. This caused a strict testing schedule to be developed, where either arm was not overused in a particular testing period.

Although a large majority of the time spent on this system was design and fabrication, validating function was just as crucial. Initially characterizing error in coordinate translation, as well as horizontal shift, allowed for the yz-projection of marker move to describe the range of motion. Not only this, translating the coordinate system to the upper arm marker allowed for the marker movement during different control modes to be in terms of a fixed coordinate system on the device itself, rather than an arbitrary origin with respect to the motion capture system.

The basic Routine mode worked as expected; illustrating one basic way that individualized robotic rehabilitation can improve traditional physical therapy. Setting the speed of motion, as well as performing the cycle many more times in a session than a PT could, clearly shows an advantage of robotic rehabilitation over traditional. Although in this particular system, the right arm brace consistently performed one cycle three-tenths of a second longer than its left counterpart. There is no clear explanation for this as there was no belt slippage during these

particular tests. Although the motors are the same model and were purchased together, one was observed to nominally spin bit faster. In practice, the Routine mode would only be used on the affected arm and the other brace would not even be worn or turned on. In this case, the slight difference in seconds per cycle would be trivial because the other brace would not be running. Furthermore, the user would be changing the speed of the routine to fit the patient's needs and additionally diminishing the issues with this discrepancy.

The graphs for the Master-Slave mode are not as smooth as those for the Routine. This is expected, since the Routine is robot controlled while Master-Slave is human controlled. Furthermore, a human is more susceptible to create stronger instantaneous torques that can lead to belt slippage, which occasionally occurred during the Master-Slave testing. More specifically, belt slippage occurred in the Left Affected Master-Slave mode when transitioning between the second and third cycles and between the 20 sec. and 25 sec. mark. This slippage is clearly shown in the Left Affected graph of Fig. 36. This is where the system would have most benefited from a better mechanism to tighten the belts.

The Master-Slave mode worked as planned with the small delay being remedied by increasing the speed of the motor to follow. It would seem like increasing the speed to follow would undoubtedly solve the problem but increasing the speed requires increasing the size of the encoder window for the following motor to fall into. As the speed increases, so does the time it takes for friction to stop the motor when it is disabled. The means that the motor could overshoot the window and actuate in reverse to fall back in. If the speed is too high and the window is not large enough, the motor oscillates back and forth outside of the range without ever landing in it. It is clear that, to avoid the lag, the speed should be increased and care should be taken on how

large the window is. If the window is too large, the motor would fall into it too far away from the desired location to stop.

Overall, the principle Myoelectric control mode took inputs and provided the correct outputs; however, the outputs were a bit delayed due to the complexity of the system code. The FPGA code was written in parallel loops, in order to not limit any independent function by another's function. This process should have been duplicated in the RT code to create producer-consumer loops or other variations of parallel processing. In this application, the RT code was written within one "while" loop, calling case structures within for each particular control mode. Unfortunately, this design paradigm leaves the entire loop dependent on the slowest function. Through development, it was thought that the parallel FPGA loops would avoid this issue, but this was not the case. From the oscilloscope images it is clear that motor actuation occurs but it begins delayed and lasts for too long. Ideally, this system would just give a burst of torque assisting- or resisting-as-needed. In reality, once the MAV is crossed and the motors actuate, they actuate until the full outer "while" loop runs. Because the speed of this loop is determined by its slowest function, the actuation occurs for too long. It must be noted that the raw EMG and the conditioned MAV are two different metrics and are very positively correlated because MAV is determined from the EMG; therefore, the raw EMG images shown with the digital output lines are not directly what initiated them. Regardless, it is clear that when the EMG is large enough, the MAV will be large enough to initiate movement.

Through stress analysis and injection molding software the feasibility of mass producing these pieces was explored. Great insight was gained here, specifically understanding how strong these plastics can actually be, and how future designs can be significantly altered to use less material.

Using the results from the Moldflow simulations, it can be determined that sub-optimal injection sites may be able to create a functioning product, but the quality will always be best from the optimal site. If an even more obscure place was chosen as the sub-optimal injection site, the simulation would have certainly returned a worse result. Furthermore, it became very clear by testing the original 3D print design that the redesign was necessary to have uniform thickness. The amount of Cooling Quality considered to be low was unacceptable and it is clear the direct reason is the difference in thickness throughout the design. It was understood from the beginning that the model needed to be redesigned to have uniform thickness and this simulation proved why.

For the stress analysis, beginning with the original 3D print designs, the peak stress was seen to be 1.934 MPa. This value corresponds to approximately 280.5 psi, far below the 7600 psi tensile strength of Polycarbonate, as seen back in Table 1. Additionally, the maximum displacement is 0.0426 millimeters which, when compared to the size of the device, will certainly have no effect on the function.

Just comparing the appearance of the two designs it´s clear the injection mold uses much less material and will have less strength. As stated the peak stress on the injection mold design was 7.145 MPa which corresponds to approximately 1036.29 psi. Although this is several times greater than the peak stress seen for the 3D printed design, it is still well below the 40 MPa or 5800 psi tensile strength for the ABS material. [36] Similarly, the largest displacement on the injection mold design was several times greater than the 0.136 millimeters seen on the 3D printed. Although the value is larger, it is still very small in relation to the device and that this amount of displacement would have no effect on the overall function.

Revisiting the fact that these tests were done on individual parts, it can now be said with confidence that this does introduce a higher level of safety because the results for the joined pieces show both a lower peak stress and lower displacement. For the illustrated injection mold design, the peak stress was 980.46 psi, less than the 1036.29 psi seen with just the Lateral Arm Support holding the motor. Similarly, the maximum displacement was 0.1019 millimeters for the joined pieces compared to 0.136 millimeters seen for just the single piece. Ultimately, through these tests it can be concluded that future designs can not only use less material, but can be formed using plastic injection molding allowing for mass production.

5.1 Future Investigations

Ultimately, the system is functional but will greatly benefit from further research and design work. In practical use, there is too much for the user to do in the Myoelectric control mode. Besides the Manual control, which is quite trivial, the other two basically require the user to simply set the control mode and observe the patient. In the Myoelectric mode, the user must constantly be monitoring the set thresholds and potentially change them as the muscle activity of the patient changes during use. More so, the user must stop and start the active assist, as well as toggle between the MVC and data acquisition, while making sure the encoder values are reset to zero and the arms are both maximally extended before restarting. As further research goes, on it will be imperative to augment the code to help the user more efficiently run this control modality.

Each mode can benefit from more advanced paradigms of control implementation. For instance, the Routine mode could be better served using a PID controller for trajectory planning with either a linear or non-linear path. Using trajectory planning would eliminate the difference

in the length of cycles seen between motors. The Master-Slave mode would be better served with a closed loop control system, in which tracking of the master brace's encoder is more than just an on/off controller. This doubles for the Myoelectric mode as well, where a closed loop PID controller would allow for the current value output from the fuzzy controller to be more accurately tracked.

In addition to augmenting or rewriting the code to make the Myoelectric control simpler to run, there are many potential areas to explore to improve the system. The bulkiness associated with a first prototype is an obvious improvement. This would include both redesigning the FDM supports and choosing a new motor and potential drivetrain. A strongly suggested improvement would be switching the pulley and timing belt system with a capstan drive. A capstan drive would allow for use of a much smaller motor with a much larger torque ratio. Not only this, many traditional haptic feedback devices use capstan drives.

The associated RT module will allow for this device to become a "headless" system in the future. Only three of the four slots in the chassis were used in the design allowing for an additional module and additional features to be incorporated. A four line digital I/O module that was purchased but only used in testing and validation may be incorporated. This digital I/O module was originally purchased to give the user some switches for controlling the "headless" system but, ultimately, the system proved too complex to run using essentially only four switches. The RT module has a D-Sub serial connector that can run up to eight digital I/O lines, so a strong suggestion would be to purchase a Reach Touchscreen from Reach Technology Inc. (Freemont, CA) or something equivalent. These touchscreens can be purchased in various sizes with various functionalities and have been proven to interface with LabVIEW. These screens

could undoubtedly assist in pulling this system away from a host computer in actual field applications.

If this system grows in complexity, EMG from more muscles could be used as inputs to the quasi-fuzzy controller. If more muscles are used, a more robust conditioning algorithm would have to be developed. For example, Lopes et al. concluded that data fusion using either a Variance Weighted Average (VWA) or a Decentralized Kalman Filter (DKF) could potentially increase the robustness of EMG extraction algorithms for myoelectric control. [18] They go on to assert advantages, such as continuous operation if an electrode has been disconnected and the possibility of including any number of electrodes into the same system. This was not useful for this application because of the necessity of connection for the limited number of electrodes. If the number of electrodes were increased, it could become beneficial.

Another potential area of exploration is biofeedback using μ-wave suppression. The μ-wave, stemming from the sensorimotor cortex, lies in the EEG frequency range of 8 to13 Hz [29]. The μ-wave rhythm reaches its maximal amplitude when an individual is at rest and it reduces through actual, imagined, or observed movement. [29] It could be explored to incorporate μ-wave suppression into the Myoelectric control mode of this project as biofeedback to the user. The μ-wave will have no direct input into the system; rather, its suppression would be shown to the user as they imagine, attempt, and then move their affected arm. This could be shown to the user in a variety of ways, perhaps using an increasing intensity of a light or possibly a thermometer-like gauge that increased as the μ-wave is suppressed. Regardless, using biofeedback to directly display the patient's intent to move could increase their effort and willingness to rehabilitate.

Throughout this period of performance, many areas to explore arose. Several of these were addressed as allowed through time and resource and, inevitably, there were many questions created to be left for further research. Whatever these uncertainties were, they gave a perspective allowing a more intelligent guess to the broader implications of this work.

6 Conclusion

The transition from traditional to robotic rehabilitation shows only promise in increasing the effectiveness of physical therapy. Robotic rehabilitation provides the ability to create a customized plan and execute it with machine precision. Not only this, the intensity and repetitiveness can be much greater than any PT could deliver by hand, more effectively stimulating motor neuron plasticity. The novel system described here aims to accomplish this task of stimulating neuron plasticity in the bicep and triceps of hemiparetic patients. This thesis presented the design and fabrication of the mechanical device, writing the software code for each control mode, integrating software to the mechanical device via a National Instruments development platform, and the validation testing of all components. The four control modes each provide a unique way to manipulate the hemiparetic arm, even giving direct control to the patient in the Master-Slave mode. The Manual and Routine modes give full control to the user of the program, much like a PT would have and finally, the Myoelectric mode surrenders control to the software but with the patient consciously providing the inputs to the system. Here the EMG signal from the patient directly determines the amount of assistance or resistance needed, providing a metric for muscle output. The muscle output is determined for both the affected and unaffected arms and is meant to guide the bilateral motions of both. As this system can be calibrated and individualized for any patient, the benefits of the transition to robotic

rehabilitation are apparent. Although this first prototype has many ways of being improved upon, the system shows a proof of concept that can be expanded and enhanced.

Annex A – Operator's Manual

Operating this device begins with choosing whether the patient is left or right side hemiparetic. The program user should always make sure to start the program in the Manual control mode. Not only this, the Manual mode should be started in the neutral toggle configuration for both arms; the flexion toggles should be down and the extension toggles should be up. Furthermore, before starting the program AND before changing to any other control mode it is imperative to make sure the braces are in the fully extended position with the encoder values reset to zero. If they are not fully extended and encoders reset to zero, not only will the control modes work incorrectly, but harm could potentially come to the patient. The program user should always return to the Manual control mode after any other mode to bring both arms back to the fully extended position and reset the encoder values to zero.

Manual Mode:

This is the mode that the program should be in before starting. This is the safest control mode to start in because it gives the program user has complete control over the braces. The program user must make sure both flexion toggles are down and both extension toggles are up to make sure nothing unexpected happens when the program is started. The program user can control flexion or extension of both arms with toggle switches on the front panel. With a pair of toggles for each arm, the user can flip the flexion toggle to initiate flexion but must flip this back down before flipping the extension toggle. If the user flips the extension toggle before returning

the flexion to its neutral down position, the system disables the motors and the program stops running. The program user can change the speed at which the braces move but should be very careful when increasing the speed. When the user and patient are ready to move on to a different control mode both braces should be lowered to fully extended positions and the encoder values reset to zero.

Routine Mode:

The Routine mode should only be run directly after the Manual control mode. It is most likely that the Routine mode will only control the hemiparetic limb, so that corresponding brace should be in the fully extended position and the encoder values reset to zero. When both the user and patient are ready, the user presses the "Start Routine" push button on the front panel. This button stays pressed and the brace begins to oscillate flexion-extension cycles. This continues indefinitely until the user presses the same button unlocking it from the pressed confirmation. The cycles stop and the user should put the program back in the Manual control mode to bring both arms to the fully extended position and reset the encoder values to zero.

Master-Slave Mode:

The Master-Slave control mode should only be operated directly after the Manual control mode. As the user has already put in which arm of the patient's is hemiparetic, the master and slave brace designations should have already been established. Once in the Master-Slave mode, the master brace immediately has control over the slave. Whether it's the patient's unaffected arm or the therapist wearing the master brace, flexion-extension movements are mimicked by the slave.

Myoelectric Mode:

First, the EMG electrodes must be placed on the biceps and triceps of both arms of the patient. These should be placed using the SENIAM guidelines described in section 2.3.1 in the body of this text. The Myoelectric control mode should only be run directly after the Manual control mode. Before entering the Myoelectric mode the program user should enter the current limit value which corresponds to the max amount torque to be provided by the motors. Also the user should again make sure that the braces are in the fully extended position, the encoder values are reset to zero, and toggle switch is in the "MVC" confirmation. When the patient and user are ready, the user switches to the Myoelectric control mode and the patient delivers their maximum voluntary contraction. When it's clear the MVC will not go any higher the user flips the toggle to "EMG Acquisition." At this point, a scrolling waveform chart displays the filtered and conditioned EMG signal and the user must subjectively set the thresholds corresponding to percent-MVC the patient must reach in each muscle. It is imperative that the user constantly monitor the scrolling waveform and adjust the threshold as needed to compensate for both muscle fatigue and errors in their original estimate. Once the patient and user are finished with the session, the user should switch back to the Manual Control mode and put the braces into the fully extended position and reset the encoder values.

7 Bibliography:

[1] Ashby D, Baker B, Hickman I. Circuit Design: Know It All. *Newnes* 2008. pp 949-955

[2] Chang J, Tung W, Wu W, Huang M, F Su. Effects of Robot-Aided Bilateral Force-Induced Isokinetic Arm Training Combined With Conventional Rehabilitation of Arm Motor Function in Patients With Chronic Stroke. *Arch Phys Med Rehabil*, vol. 88 pp. 1332-38. 2007.

[3] Clancy EA, Bouchard S, Rancourt D. Estimation and application of EMG amplitude during dynamic contractions. *IEEE Eng. Med. Biol. Mag.*, vol. 20, no. 6, pp 47-54. 2001

[4] Day S. Important Factors in Surface EMG Measurment. Bortec *Biomedical Ltd*. 225, 604-1st st SW Calgary, AB, Canada.

[5] Delsys, Products. Accessed February 17th, 2012. <http://delsys.com/Products/Products.html>

[6] Englehart K, Hudgins B. A Robust, Real-Time Control Scheme for Multifunction Myoelectric Control. IEEE *Transactions of Biomedical Engineering*, vol. 50, no. 7, pp 848-854. 2003.

[7] Farina D, Merletti R, Enoka RM. The extraction of neural strategies from the surface EMG, *J. Appl. Physiol*., vol 96, pp 1486-1495. 2004.

[8] Gladstone DJ, Danells CJ, Black SE. The Fugl-Meyer Assessment of Motor Recovery after Stroke: A Critical Review of Its Measurement Properties. *Neurorehabilitation and Neural Repair*, vol. 16, pp 232-240. 2002.

[9] Groce CM. Hemiparesis. *National Stroke Association*. Accessed 15 October 2011, <http://www.stroke.org/site/PageServer?pagename=hemiparesis>.

[10] HemiHelp: For Children and Young People with Hemiplegia. Accessed 18 October 2011, <www.hemihelp.org.uk>.

[11] Hemiplegia Symptoms, Treatment and Therapy. Accessed 18 October 2011, <http://hemiplegiatreatment.net>

[12] Introduction to LabVIEW FPGA – Webcasts and Videos. Accessed 14 April 2012 http://zone.ni.com/wv/app/doc/p/id/wv-229

[13] Introduction to LabVIEW Real-Time – Webcasts and Videos. Accessed 14 April 2012, http://zone.ni.com/wv/app/doc/p/id/wv-1349

[14] Khezri M, Mehran J. Reat-time intelligent pattern recognition algorithm for surface EMG signals. *BioMedical Engineering OnLine*, vol. 6, no. 45. 2007.

[15] Kiguchi K, Imada Y, Liyanage M. EMG-Based Neuro-Fuzzy Control of a 4DOF Upper-Limb Power-Assist Exoskeleton. *Proceedings of the 29th Annual International Conference of the IEEE EMBS*, 2007 August 23-26, Lyon, France.

[16] Li G, Li Y, Yu L, Geng Y. Conditioning and Sampling Issues of EMG Signals in Motion Recognition of Multifunctional Myoelectric Prosthesis. *Annals of Biomedical Engineering*, vol. 39, no. 6, pp. 1779-1787. 2011.

[17] Liao W, Wu C, Hsieh Y, Lin K, Chang W. Effects of robot-assisted upper limb rehabilitation on daily function and real-world arm activity in patients with chronic stroke: a randomized trial. *Clinical Rehabilitation*, vol. 0, no. 0, pp. 1-10. 2011.

[18] Lopez NM, Sciascio F, Soria CM, Valentinuzzi ME. Robust EMG sensing system based on data fusion for myoelectric control of robotic arm, *BioMedical Engineering OnLine*, vol. 8, no. 5. 2009.

[19] Marchal-Crespo L, Reinkensmeyer DJ. Review of control strategies for robotic movement training after neurologic injury. *Journal of NeuroEngineering and Rehabilitation*, vol. 6 no 20. 2009.

[20] Masiero S, Celia A, Rosati G. Armani M. Robotic-Assisted Rehabilitation of the Upper Limb After Acute Stroke. *Arch Phys Medical Rehabil*, vol. 88 pp 142-149. 2007.

[21] Merletti R., Parker P. Electromyography - Physiology, Engineering, and Noninvasive Applications. *John Wiley & Sons*. pp. 1-25,259-304,435-451,453-475. 2004.
Online version available at:
<http://www.knovel.com/web/portal/browse/display?_EXT_KNOVEL_DISPLAY_bookid=1965&VerticalID=0>.

[22] Mudie, MH, Matyas TA. Can simultaneous bilateral movement involve the undamaged hemisphere in reconstruction of neural networks damaged by stroke? *Disability Rehabilitation*, vol. 22, pp 23-37. 2000.

[23] Nijland R, Kwakkel G, Bakers J, van Wegen E. Constraint-induced movement therapy for the upper paretic limb in acute or sub-acute stroke: a systematic review. *International Journal of Stroke*, vol. 6, pp 425-433. 2011.

[24] NI LabVIEW FPGA Module – National Instruments. Accessed 14 April 2012, http://www.ni.com/fpga/

[25] NI LabVIEW Real-Time Module – National Instruments. Accessed 14 April 2012, http://www.ni.com/labview/realtime/

[26] Oskoei MA, Hu, H. Myolectric control systems – *A survey. Biomedical Signal Processing and Control*, vol. 2, pp. 275-294. 2007.

[27] Page SJ, Sisto S, Levine P, Johnston MV, Hughes M. Modified constraint induced therapy: A randomized feasibility and efficacy study. *Journal of Rehabilitation Research and Development*, vol. 38, no. 5. pp 593-590. 2001.

[28] Passino KM, Yurkovich S. Fuzzy Control. *The Ohio State University Department of Electrical Engineering*. 1998.

[29] Pineda JA, Giromini L, Porcelli P, Parolin L, Viglione DJ. Mu suppression and human movement responses to the Rorschach test. *NeuroReport*, vol. 22, no. 5, pp 223–226, 2011.

[30] Poon CS. Sensorimotor learning and information processing by Bayesian internal models. Proceedings of the 26th Annual International *Conference of IEEE Engineering in Medicine and Biology Society, IEMBS*, vol. 4 pp 4481-4482, 2004.

[31] Quickparts, Learning Center/BasicsofInjectionMoldingDesign. Accessed 12 July 2013, <www.quickparts.com/LearningCenter/BasicsofInjectionMoldingDesign.aspx>

[32] Quickparts, Low-Volume/Prototypes, FDM. Accessed 11 March 2012, <www.quickparts.com/LowVolumePrototypes/FDM.aspx>

[33] Quickparts, Low-Volume/Prototypes, SLA. Accessed 11 March 2012, <www.quickparts.com/LowVolumePrototypes/SLA.aspx>

[34] Rossini PM, Dal Forno G. Integrated technology for evaluation of brain function and neural plasticity. *Phys Med Rehabil Clin N AM*, vol. 15, no. 1, pp 263-306. 2004.

[35] Whitall J, McCombe SW, Silver KH, Macko RF. Repetitive bilateral arm training with rhythmic auditory cueing improves motor function in chronic hemiparetic stroke. *Stroke*, vol. 31, pp 2390-2395. 2000.

[36] Xahax. ABS Material. Accessed 12 July 2013, < xahax.com/subory/Spec_ABS.pdf>

[37] Zecca M, Micera S, Carrozza MC, Dario P. Control of Multifunctional Prosthetic Hands by Processing the Electromyographic Signal. *Critical Reviews in Biomedical Engineering*, vol. 30, pp 459-485. 2002.